






Use of Decellularized SMILE (Small-Incision Lenticule Extraction) Lenticules for Engineering the Corneal Endothelial Layer: A Proof-of-Concept

Swatilekha Hazra, Jacquelyn Akepogu, Supriya Krishna, SriRavali Pulipaka, Bhupesh Bagga & Charanya Ramachandran

To cite this article: Swatilekha Hazra, Jacquelyn Akepogu, Supriya Krishna, SriRavali Pulipaka, Bhupesh Bagga & Charanya Ramachandran (2022): Use of Decellularized SMILE (Small-Incision Lenticule Extraction) Lenticules for Engineering the Corneal Endothelial Layer: A Proof-of-Concept, Current Eye Research, DOI: [10.1080/02713683.2022.2151018](https://doi.org/10.1080/02713683.2022.2151018)

To link to this article: <https://doi.org/10.1080/02713683.2022.2151018>

 View supplementary material 

 Published online: 02 Dec 2022.

 Submit your article to this journal 

 View related articles 

 View Crossmark data 



Use of Decellularized SMILE (Small-Incision Lenticule Extraction) Lenticules for Engineering the Corneal Endothelial Layer: A Proof-of-Concept

Swatilekha Hazra^{a,b}, Jacquelyn Akepogu^{a,b}, Supriya Krishna^{a,c}, SriRavali Pulipaka^{a,d}, Bhupesh Bagga^e, and Charanya Ramachandran^a

^aProfessor Brien Holden Eye Research Centre, LV Prasad Eye Institute, Hyderabad, Telangana, India; ^bManipal Academy of Higher Education, Manipal University, Manipal, India; ^cLudwig-Maximilians University, Munich, Germany; ^dDepartment of Applied Biology, CSIR-Indian Institute of Chemical Technology, Hyderabad, Telangana, India; ^eDepartment of Cornea and Anterior Segment, LV Prasad Eye Institute, Hyderabad, Telangana, India

ABSTRACT

Purpose: To demonstrate the suitability of using decellularized SMILE (Small-incision Lenticule Extraction) lenticules for culturing and transplanting the corneal endothelium (CE).

Methods: The SMILE lenticules, obtained during refractive surgery, were decellularized by incubating in CE culture medium and fetal bovine serum. Decellularization was confirmed by hematoxylin and eosin staining, DAPI staining, and gel electrophoresis. The amount of DNA per milligram of dry tissue weight was calculated to quantify the residual nuclear content. The transparency of the decellularized lenticules was determined by calculating the modulation transfer function. Immunostaining for stromal collagens and glycosaminoglycan was performed using specific antibodies. Engineered tissue was constructed by culturing the CE cells on lenticules and staining for ZO-1, Na/K ATPase, and N-cadherin. The functionality of the engineered tissues was assessed by transplanting them onto edematous human donor corneas and perfusing for 10 days *ex-vivo*.

Results: The residual DNA per milligram of dry tissue weight was found to be significantly reduced ($p < 0.0001$) in serum (0.255 $\mu\text{g}/\text{mg}$) and Opti-MEM (0.140 $\mu\text{g}/\text{mg}$) when compared to fresh lenticules (3.9 $\mu\text{g}/\text{mg}$). Decellularization did not alter the arrangement of the collagen fibers or the transparency of the lenticules. CE cells attached and matured to express ZO-1, Na/K ATPase, and N-cadherin at two weeks after seeding. The engineered tissue upon transplantation significantly reduced the corneal edema ($p < 0.05$) and the transplanted cells remained intact on the SMILE lenticule post-transplantation.

Conclusion: This study demonstrates the suitability of using SMILE lenticules decellularized using a simple, chemical-free method for engineering the corneal endothelium for transplantation.

ARTICLE HISTORY

Received 24 June 2022

Accepted 19 November 2022

KEYWORDS

Decellularization; SMILE lenticules; tissue engineering; transplantation; corneal endothelium

Introduction

The cornea is one of the most transplanted tissues globally, accounting for ~180,000 surgeries in a single year in over 116 countries. Yet, only 1 healthy tissue is available for every 70 that are required leaving nearly 12.7 million people awaiting transplantation.¹ Of the total corneal transplants performed in a given year, nearly 40% of them are done to replace the dysfunctional corneal endothelium (CE).² Engineering the endothelial layer, therefore, would provide a much-needed alternative to donor tissues. Tissue engineering involves two important steps: the first is the generation of the native cells and the second is the material used to construct the tissue. Many synthetic and biological materials have been used for constructing the CE layer.^{3–9} Of particular interest is the corneal stroma since it retains all the required features of the native tissue allowing for better integration after transplantation. In recent times, lenticules that

are extracted during refractive surgery (Small Incision Lenticule Extraction or SMILE) have garnered interest since they provide a cadaver-donor independent source of corneal stroma and are readily available. These lenticules are increasingly being used as implants to correct hyperopia,^{10,11} presbyopia,^{12,13} as grafts to treat tears/perforations^{14–16} and for constructing corneal equivalents.^{17,18}

For tissue engineering, the biological source must be decellularized because the presence of residual cellular material can trigger the immune system to reject the transplantation or can affect the remodeling following transplantation.^{19,20} While ensuring sufficient decellularization, it is also important to retain much of the native extracellular matrix (ECM), which is known to regulate cell mitogenesis, differentiation and can induce host tissue remodeling.^{21–23} In the case of corneal transplantation, the tissue transparency must also be unaffected following decellularization. Several chemical (e.g. detergents), enzymatic (e.g. collagenase, trypsin), and physical

methods (e.g. compression, freeze-thawing) have been used to decellularize human and animal corneal tissues.^{18,24–35} The efficacy of these techniques at removing cellular components varies with tissue thickness but the most common drawbacks reported are the stripping of ECM proteins, compromised optical clarity, and a loss in the tensile strength of the tissue. Further, the residual presence of any of the chemicals used for decellularization can evoke an adverse immune response after transplantation thus requiring extensive washing over several hours or days.

In this paper, we report a simple, chemical-free, yet effective technique for decellularizing the SMILE lenticules, which were used for engineering the human CE (hCE) layer. The engineered hCE layer, when transplanted to the human cornea using an *ex-vivo* perfusion system, was able to significantly reduce corneal edema thus providing proof for its potential use as a carrier for transplanting cultured hCE cells.

Materials and methods

Materials

Opti-MEM and keratinocyte media (KM) were purchased from Gibco, Thermo fisher Scientific, USA. Fetal bovine serum (FBS) was from Hyclone; chondroitin sulfate and calcium chloride were from Sigma, USA. Epidermal growth factor, insulin, gentamicin, phalloidin, anti-mouse IgG, anti-rabbit IgG, live-dead assay kit (R37601), and anti-ZO-1 antibody were purchased from Invitrogen, USA. NaCl and Cell Tracker Red CMTPX (C34552) were from Thermo fisher Scientific, USA. DNase was purchased from Promega, USA. Collagens 1, 3, 5, 12, anti-keratan sulfate, anti-Na/K ATPase, and anti-N-cadherin antibodies were from Santa Cruz Biotechnology, USA. Collagen 3 antibody was from Abcam, UK, and collagen 4 antibody was from GENEXT Genomics Pvt. Ltd., India. The antibody details are provided in [supplementary table 1](#).

Preparation of SMILE lenticules

Stromal lenticules were obtained from patients undergoing SMILE refractive surgery after obtaining institutional review board approval (LEC 07-17-067) and informed consent. A total of 160 lenticules were collected for the study with an average thickness of $84.519 \mu\text{m} \pm 29.2 \mu\text{m}$ and a diameter of 6.5 mm for all lenticules. The lenticules were rinsed with 0.05% betadine followed by a wash with 1X phosphate-buffered saline (PBS) and then were placed in the following media for decellularization (1) CE medium (Opti-MEM, 8% FBS, 0.08% chondroitin sulfate, 200 mg/L calcium chloride, 5 ng/ml EGF, 50 $\mu\text{g}/\text{ml}$ gentamicin), (2) keratinocyte medium (DMEM + F12, 10% FBS, 5 ng/ml EGF, 5 mg/ml insulin, 50 $\mu\text{g}/\text{ml}$ gentamicin), (3) fetal bovine serum, and (4) 1X phosphate-buffered saline. Lenticules decellularized using 1.5 M NaCl + 5U DNase as per the previous protocol with some modifications served as the positive control.¹⁸ Briefly, for NaCl-DNase treatment, 1.5 M NaCl was added to

the lenticules for 24 hrs, removed, and replaced with fresh solution for an additional 24 hrs. The NaCl solution was removed and 5 units of DNase were added to the lenticules and incubated for 24 hrs. After removal of the DNase, the lenticules were washed in 1xPBS for 24 hrs followed by 3 washes in 1xPBS for 5 mins each. Fresh lenticules and lenticules placed in KM served as negative controls. Following incubation in the different media for the specified time points, the lenticules were taken for further assessment.

DAPI staining of lenticules

After treatment, the lenticules were stained with 4', 6-diamidino-2-phenylindole (DAPI) for 5 mins, followed by three PBS washes of 5 mins each. The lenticules were mounted using glycerol and images were taken at 5X magnification using the Zeiss Airyspace LSM 880 confocal microscope. The images were stitched together to create montages of the lenticules.

Live-dead assay

The end-point of decellularization was 7 days for Opti-MEM medium (37 °C), 1X PBS (4 °C) and KM (37 °C), and 72 hrs for FBS (37 °C). The assay was conducted at 24 hrs for comparison. NaCl-DNase treated lenticule was used as the control for decellularization and fresh lenticules served as the negative control. After incubation in the respective media for the defined time points, the lenticules were washed with 1X PBS and checked for keratocyte viability using LIVE-DEAD cytotoxicity assay as per the manufacturer's recommendations. Images were taken at 10X magnification using the Zeiss Airyspace LSM 880 confocal microscope. Live and dead cells at the end time point of each treatment were quantified by calculating the corrected total cell fluorescence (CTFT) using Image J software. The intensity values for green and red fluorescence were quantified based on the formula: $\text{CTFT} = \text{Integrated density} - (\text{area of selected cells} \times \text{background mean gray value})$. Images from four different fields and depths of lenticules were taken for quantification. The quantification was conducted on two biological replicates ($N = 2$). One-way analysis of variance (ANOVA) with Tukey's multiple comparisons test was performed on the data using GraphPad Prism V9.0 and $p \leq 0.05$ was considered statistically significant.

DNA extraction and quantification

Lenticules, at the end of the incubation period in the different media, were dried at 60 °C for 2 hrs and the dry weight of the lenticules was measured. Dried lenticules were chopped and suspended in 200 μl of lysis buffer containing 1 M Tris pH 8, 10% SDS, and 0.5M EDTA pH 8. After 10 mins of incubation at room temperature, 20 mg/ml Proteinase K (Genei, India) was added and incubated at 56 °C for 2 hrs. 10 μl of 5M NaCl and equal proportions of isopropanol were added and incubated at 4 °C for 10 mins and centrifuged at 12,000 rpm for 15 mins. The supernatant

was removed followed by resuspension of the pellet in 70% ethanol and centrifugation at 12,000 rpm for 5 mins. Ethanol was discarded and the air-dried pellet was resuspended in TE buffer (pH 8). DNA was quantified using NanoDrop (Thermo Scientific, USA) and the values were used to calculate DNA concentration per milligram weight of lenticules ($N=3$). One-way analysis of variance (ANOVA) with Tukey's multiple comparisons test was performed on the data using GraphPad Prism V9.0. Significance was set at $p < 0.05$. Agarose gel electrophoresis was used to visualize the genomic DNA.

Fluorescence staining

The paraffin-embedded sections of fresh lenticule, lenticules placed in PBS for 7 days, Opti-MEM for 7 days, in serum for 72 hrs, and NaCl-DNase treated lenticules were first deparaffinized by heating at 70 °C for 2–5 mins, followed by three xylene washes of 5 mins each, and serial ethanol wash of 100, 90, and 80% for 5 mins each. Antigen retrieval was performed by heating the samples in sodium citrate buffer for 15 mins, followed by staining for specific stromal collagens 1, 3, 4, 5, 12, and keratan sulfate (glycosaminoglycan marker). Lenticule sections stained only with the secondary antibody of mouse and rabbit were used as the control for quantification (Supplementary Figure 1). The intensity of collagen proteins across all the groups was compared by calculating the CTFT value, as described in the earlier section, using Image J software, NIH. The total intensity obtained for each group was subtracted from the intensity obtained for the negative control. Two sections for each treatment condition were used for the quantification of total fluorescence.

To check for residual cytoskeletal components after decellularization, the lenticules were fixed with 4% paraformaldehyde for 10 mins at room temperature, rinsed thrice with PBS, and incubated in 0.1% Triton-X for 5 mins. Next, the cells were incubated in 1:200 diluted phalloidin, washed in PBS, counterstained with DAPI, and imaged using the Zeiss Airyscan LSM 880 confocal microscope. The total intensity for phalloidin staining was quantified from five images at different depths using Image J software, NIH, and plotted to determine the decrease in residual cytoskeletal components in the treated groups. Fresh lenticule was used as the control for comparison. One-way analysis of variance (ANOVA) with Tukey's multiple comparisons test was performed, and $p \leq 0.05$ was considered statistically significant.

Hematoxylin and eosin staining

Sections at the initial time point of 24 hrs and end time points of PBS (7 days), Opti-MEM (7 days), Serum (72 hrs), KM (7 days), and NaCl-DNase were stained with hematoxylin-eosin (H&E) to determine the presence of cells in the lenticules and periodic acid-Schiff base (PAS) staining to visualize collagen.

The thickness of the lenticules was quantified from the H&E sections using the ZEN 3.5 Blue Edition software,

Zeiss. Five measurements of the central thickness were taken per lenticule for each treatment group and from two tissue sections each. The results are reported as mean \pm SD. One-way analysis of variance (ANOVA) with Tukey's multiple comparisons test was performed, and a p -value ≤ 0.05 was considered statistically significant.

Scanning electron microscopy

The structure of the collagen fibers in the treated lenticules was visualized using scanning electron microscope (SEM). The samples were fixed in 4% glutaraldehyde in cacodylate buffer of 7.4 pH for 24 hrs. They were then treated with 1% osmium tetroxide, followed by three washes using distilled water. Samples were then dehydrated with alcohol in ascending order of 10, 30, 50, 70, and 90% for 20 mins each, followed by 100% alcohol for 20 mins twice. They were then dried at room temperature overnight, gold-sputtered, and imaged using Zeiss EVO 18 microscope.

Optical performance of lenticules

The optical performance of the wet lenticules was determined using two-dimensional modulation transfer function (MTF) using MATLAB software (Nantucket, MA, USA) as reported earlier.⁸ In-focus and blurred images of the letters "LVP" without any lenticules were used as controls. The normalized power values were plotted as a function of the object frequency. It is expected that in a natural scene, the optical performance will reduce with an increase in object spatial frequency. The analysis determined if the MTF loss with the decellularized lenticules was any greater than or equal to the MTF loss without lenticule.

Human corneal endothelial cell culture on lenticules

Donor corneas, unsuitable for transplantation, were obtained from the Ramayamma International Eye Bank, LV Prasad Eye Institute, Hyderabad, India and handled according to the declaration of Helsinki. The corneas were harvested within 24 hrs of death, preserved in McCarey-Kaufman medium, and used within 4 days of preservation. Cells from 3 donors of ages 1 month, 4.5 months, and 2 years were used for primary cell culture. Details of the donor tissues are included in supplementary table 2. The isolation and culture of hCE cells followed the reported methods.^{8,36} Briefly, donor tissues were disinfected by washing in PBS containing antibiotics, and Descemet's membrane along with the CE cells was gently peeled. The peeled tissues were chopped into smaller pieces and digested using collagenase (1 mg/ml) for 2–6 hrs. The cells were dissociated using trypsin-EDTA (0.25%) and then seeded on fibronectin and collagen 1 (FNC)-coated dishes. The culture medium was changed every 2 days until the cells reached confluence and then subcultured by trypsinization. Cells between passages 1 and 3 were seeded at 3000 cells/mm² on fresh SMILE lenticules for 2 weeks and stained for phalloidin, N-cadherin, Na/K

ATPase and ZO-1 following which imaging was done using Zeiss Airyscan LSM 880 confocal microscope.

Ex-vivo perfusion

Cells between passages 1 and 3 were seeded on lenticules at a density of 3000cells/mm² and cultured for 3 days before transplantation. The cells were stained with Cell Tracker Red CMTPX Dye (10μM) for 45 mins before transplantation. The recipient donor corneas were rinsed thoroughly with PBS and the existing CE cells were removed by incubating in trypsin-EDTA (0.25%) and gently washing the loosened cells. Removal of the cells was confirmed using trypan blue staining after which they were placed in Opti-MEM overnight to induce swelling. The corneal thickness was measured using optical coherence tomography (OCT) before transplantation. The lenticules with or without hCE cells were then carefully transplanted into the donor corneas. Fibrin glue was used to aid with the adhesion of the lenticule to the posterior cornea. The corneas along with the lenticules were mounted onto the artificial anterior chamber connected to a peristaltic pump to maintain a constant flow rate of 2.5μl/min and pressure of 15 mmHg. This setup was placed in a CO₂ incubator and constantly perfused with Opti-MEM medium. The perfusion setup is similar to that used by Patel *et al.*, for injecting CE cells with magnetic beads.³⁷ Silicone oil (PDMS 10 cc 5000 centiStokes (cSt),

Micromed, Italy) was added on top of the epithelial surface to reduce the evaporation of media through the anterior cornea. Central corneal thickness was measured 10 days after perfusion using OCT. The experiments were repeated twice ($N=3$) and the results are reported as mean \pm SD. Student's *t*-test was performed using Graphpad prism software and a *p*-value ≤ 0.05 was considered to be statistically significant. Details of the donor corneas used for perfusion are given in [supplementary table 3](#).

Results

Decellularization of lenticules

Fresh lenticules placed in Opti-MEM medium, PBS, and KM for different time points (24 hrs, 48 hrs, 72 hrs, and 7 days) were fixed and stained with DAPI to determine the presence of nuclear material ([Figure 1](#)). There was no perceptible difference in DAPI staining at 24 hrs but a reduction in keratocytes was obvious at 48 hrs in lenticules placed in Opti-MEM ([Figure 1\(B\)](#)). By 7 days, the nuclear material was not visible in lenticules placed in Opti-MEM unlike PBS and KM ([Figure 1\(D vs. H and L\)](#)), and was comparable to NaCl-DNase ([Figure 1\(P\)](#)). Changing the temperature of the medium from 37 to 4°C or PBS from 4 to 37°C did not alter the results. Similarly, agitation of lenticules (200 rpm) for 48 hrs did not hasten the degradation or removal of the nuclear material (data not shown).

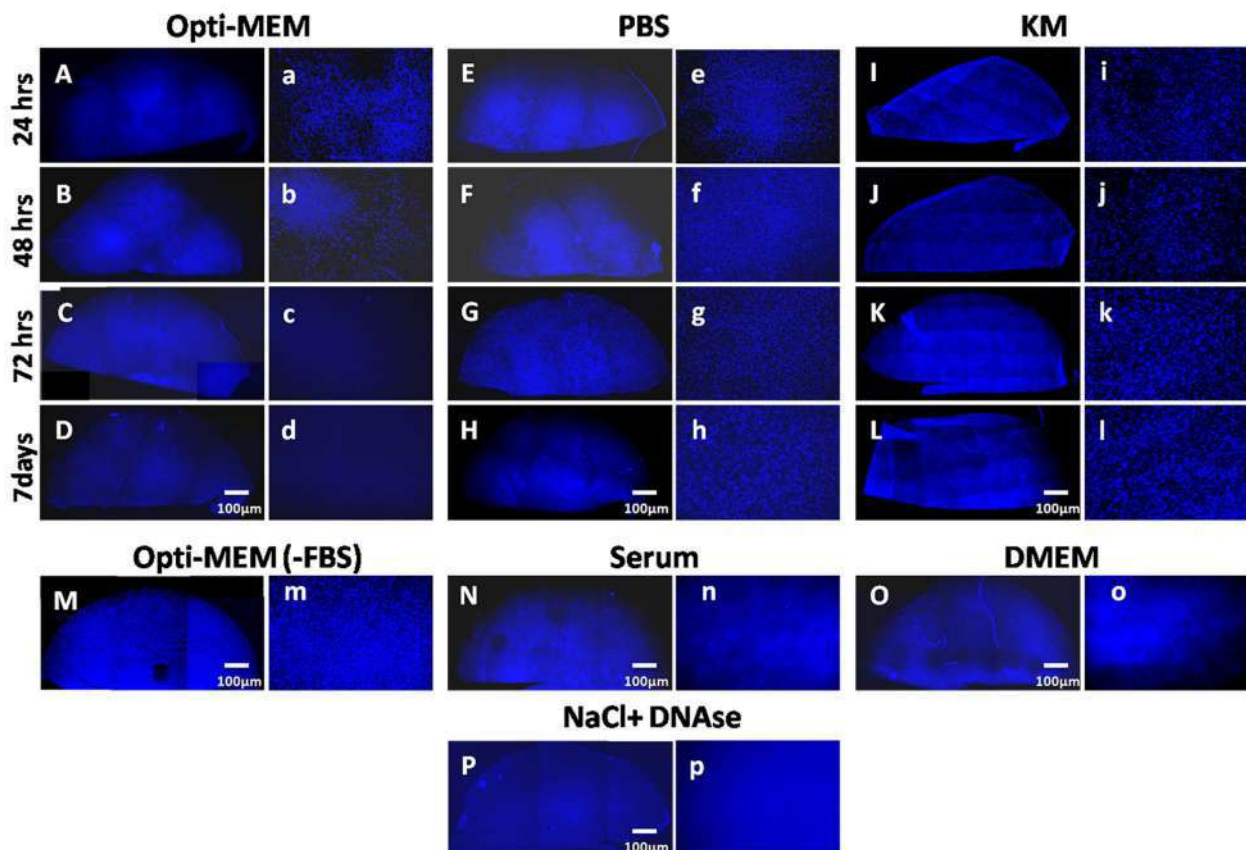


Figure 1. DAPI staining showing the presence of cell nuclei in lenticules.

Next, we wanted to check the component in the Opti-MEM medium that degraded the nuclear components. A few lenticules were placed in Opti-MEM medium without serum. As shown in Figure 1(M), there was significant nuclear staining visible even after 7 days. Therefore, we narrowed the effect of decellularization to serum in the medium. To confirm, lenticules were incubated in 100% serum which resulted in a significant reduction in DAPI staining (Figure 1(N)) within 72 hrs. Decellularization of the lenticule was also seen in those placed in DMEM containing 2% serum for 7 days (Figure 1(O)).

Decellularization was further confirmed using H&E staining of the tissue sections after incubation in the respective media until the endpoint as shown in Supplementary Figure 2. Nuclei could not be detected in sections from lenticules placed in Opti-MEM for 7 days, serum for 72 hrs or treated with NaCl-DNase (Supplementary Figures 2(E,G,I)) unlike fresh lenticules, lenticules placed in PBS for 7 days or in KM for 7 days (Supplementary Figures 2(A,C,H)) further confirming the results in Figure 1.

Incubation in Opti-MEM resulted in cell death

As expected, cells in lenticules placed in KM were viable at both 24 hrs and 7 days as can be seen in Figures 2(A,F). More dead cells could be appreciated in lenticules that were placed in Opti-MEM even at 24 hrs when compared to KM (Figure 2(C vs. A)). At 7 days, there were no viable cells left in these lenticules and the staining for dead cells was also scarce indicating that the degraded nuclear material was also removed (Figure 2(H)). Lenticules placed in serum showed extensive cell death at 72 hrs (Figures 2(D,I)) and those placed in PBS also had many dead cells at 24 hrs (Figure 2(B)) which significantly increased by 7 days (Figure 2(G)) but the degraded nuclei were still visible. Lenticules treated with NaCl-DNase were almost devoid of live cells (Figure 2(J)) which was the opposite of fresh lenticules (Figure 2(E)) in which the dead cells were very scarce. Quantification of fluorescence intensity of live and dead cells in these lenticules showed a significant reduction in the live cells in lenticules treated with Opti-MEM, serum, or NaCl-DNase when compared to fresh lenticules or lenticules incubated in KM

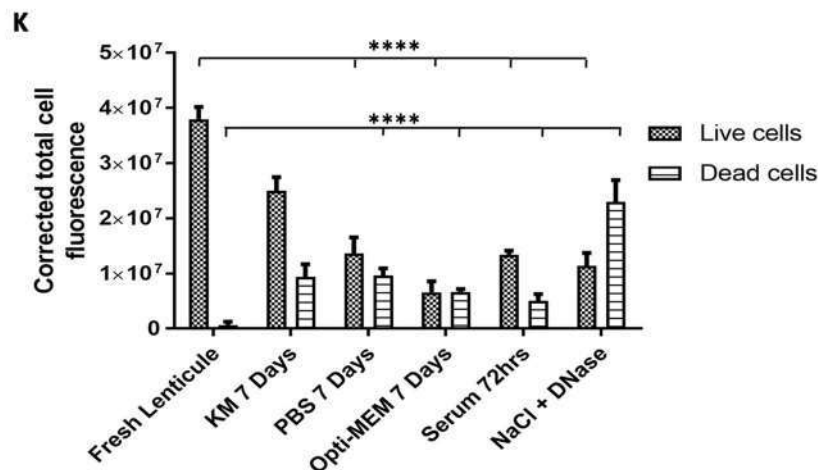
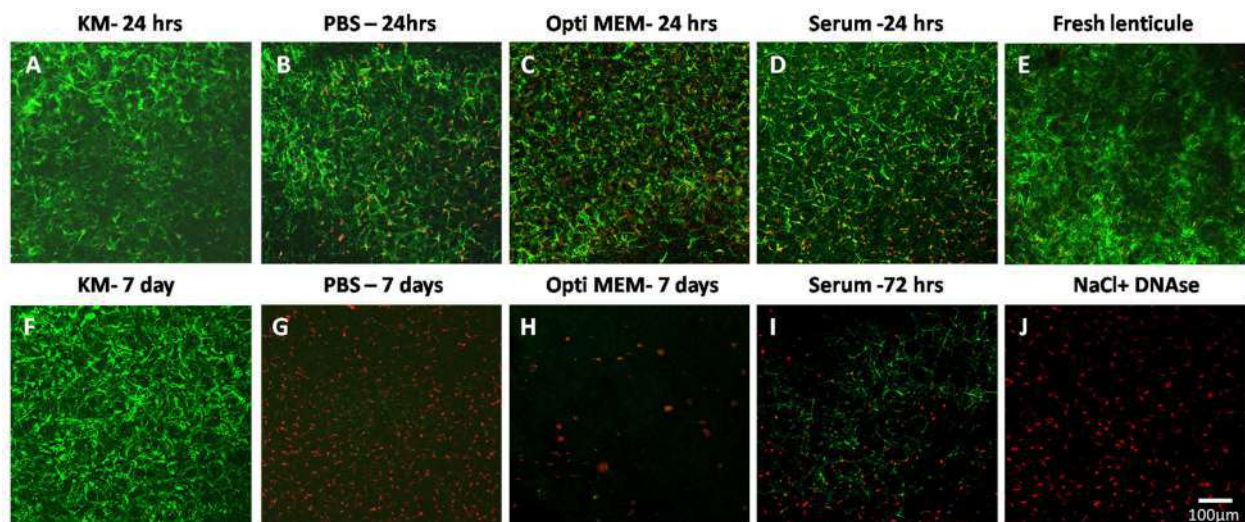


Figure 2. Live-dead imaging of decellularized lenticules.

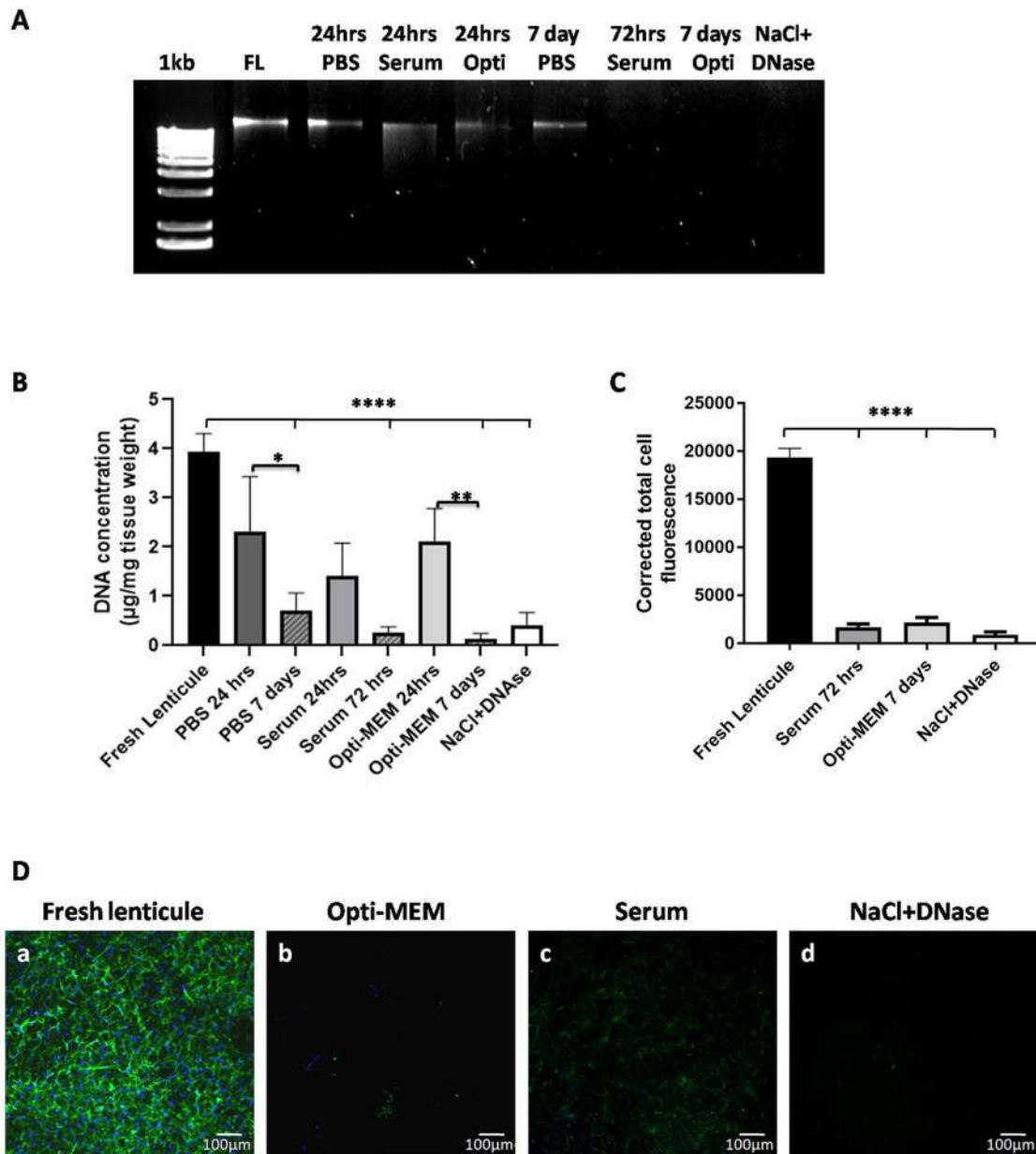


Figure 3. Quantification of residual DNA.

(Figure 2(K)). Contrarily, the staining for dead cells was significantly more in those treated with NaCl-DNase when compared to fresh lenticules, Opti-MEM, or serum (Figure 2(K)) indicating the presence of residual degraded DNA in these lenticules.

Quantification of residual DNA content

Genomic DNA was seen in fresh lenticule, PBS, serum, and Opti-MEM at 24 hrs. At 7 days, DNA was still present in lenticules placed in PBS (Figure 3(A)). However, no bands were observed in the case of 7 days Opti-MEM, serum, and NaCl-DNase treated lenticules (Figure 3(A)).

Calculation of the residual DNA per milligram dry weight of the lenticules indicated a reduction in the following order: 7 days Opti-MEM > 72 hrs serum > NaCl-DNase > 7 days

PBS (Figure 3(B)). The decellularization obtained with serum and Opti-MEM at the respective endpoints was comparable to NaCl-DNase and there was no significant difference between these methods. Though not statistically significant, the DNA in lenticules placed in Opti-MEM (0.149 µg/mg) was much lower when compared to NaCl-DNase (0.419 µg/mg) or PBS (0.718 µg/mg) and comparable to serum (0.255 µg/mg).

Next, we wanted to check the effect of the decellularization technique on the cytoplasmic cell contents. Positive staining for actin cytoskeleton indicated the presence of keratocytes in fresh lenticules. There was a significant reduction ($p \leq 0.0001$) in actin staining in lenticules placed in serum (72 hrs) and Opti-MEM (7 days) which was comparable to NaCl-DNase treated lenticules indicating substantial removal of cell cytoplasm along with nuclear components (Figure 3(C,D)).

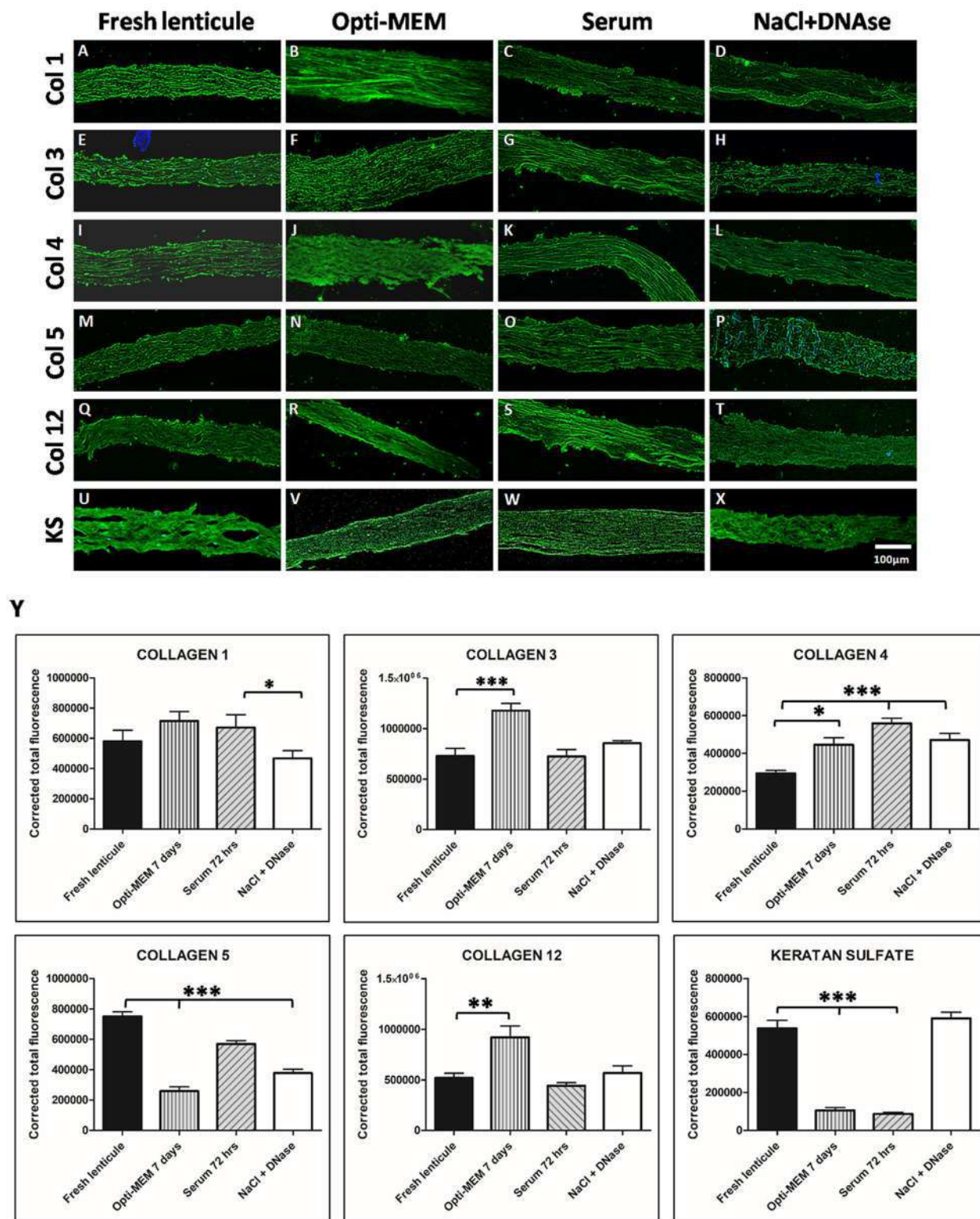


Figure 4. Immunostaining for ECM and GAG proteins.

ECM preservation in the treated lenticules

Lenticule sections were immunostained for corneal stroma-specific collagens (collagens 1, 3, 4, 5, and 12) and keratan sulfate at the respective endpoints for serum and Opti-MEM. The lenticules showed positive expression for all the markers indicating that there was no detectable loss of

collagens (Figure 4(A-T)) or glycosaminoglycans (Figure 4(U-X)) following decellularization. Quantification of the fluorescence intensity showed that there was no significant loss of collagen 1 in Opti-MEM and serum-treated lenticules unlike NaCl-DNase-treated lenticules ($p < 0.05$) when compared to fresh lenticule. There was a significant reduction in

collagen 5 in all the treated lenticules compared to fresh lenticule ($p < 0.01$) indicating a loss of this collagen protein following decellularization (Figure 4(Y)). On the contrary, there did not seem to be any loss of collagens 3 and 12 in serum and NaCl-DNase-treated lenticules compared to control however, there was increased expression of the same in Opti-MEM treated lenticules (Figure 4(Y)). Interestingly, there was an increase in collagen 4 expression in all the treated lenticules compared to the control ($p < 0.05$ for control vs. Opti-MEM; $p < 0.001$ for control vs serum and NaCl-DNase). On the contrary, there was a significant decrease in the expression of the glycoprotein, keratan sulfate, in Opti-MEM and serum lenticules and surprisingly no loss in NaCl-DNase-treated lenticules (Figure 4(Y)).

PAS staining showed intact and homogenous collagen fibers in fresh lenticules, Opti-MEM 7 days, FBS 72 hrs, and KM 7 days (Supplementary Figures 2(a,e,g,h)). Disruption in the collagen fibers could be noted in PBS 7 days and NaCl-DNase treated lenticules (Supplementary Figures 2(c,i)). Scanning electron microscope images showed no difference in the structure of collagen fibers in the treated groups of PBS, KM, serum, and Opti-MEM when compared to the fresh lenticule (Supplementary Figure 3). In NaCl-DNase treated lenticule, large gaps could be noted indicating some loss in the ECM structure (arrows in Supplementary Figure 3).

Thickness of lenticules

The thickness of the lenticules was measured using the H&E stained sections of the lenticules at the respective endpoint of incubation in PBS (7 days), Opti-MEM (7 days), Serum (72 hrs), KM (7 days), and NaCl-DNase. The thickness significantly increased in PBS ($112.6 \pm 5 \mu\text{m}$) and Opti-MEM ($117.1 \pm 5 \mu\text{m}$) when compared to fresh lenticules ($96.3 \pm 5.7 \mu\text{m}$) and was comparable to KM ($111.13 \pm 13.6 \mu\text{m}$; Supplementary Figure 4). No significant difference in thickness was observed between 72 hrs of serum and fresh lenticule. However, a significant reduction in thickness was observed in NaCl-DNase-treated lenticules ($77.5 \pm 5.5 \mu\text{m}$) compared to fresh lenticule, Opti-MEM, and serum (Supplementary Figure 4).

Optical performance of decellularized lenticules

The optical performance of the lenticules was measured as their ability to transmit information from the object to the image with high fidelity. It is expected that swelling would greatly reduce transparency which would, in turn, affect the optical performance of the decellularized tissues. Modulation transfer function or MTF is a good measure of the effective resolution of the image which can be degraded by blur. At higher spatial frequencies the MTF reaches 0 which indicates poor visibility of smaller structures. At lower spatial frequency, the MTF is near 1 indicating the ability to visualize larger structures. A decrease in the object contrast (in this case due to loss of lenticule transparency) can reduce the image contrast resulting in degradation of information

reflecting on the optical clarity of the lenticule. The MTF values were calculated for fresh lenticule, 72 hrs serum, 7 days KM, 7 days Opti-MEM, and NaCl-DNase treated lenticules. A focused high-resolution image of the object served as the positive control while an optically blurred image served as the negative control (Figure 5(A,B)). As expected, the performance of the lenticules decreased at higher object spatial frequencies. However, this decrease was comparable to the fresh lenticule indicating that there was no degradation of information induced by the decellularization process (Figure 5(C)) confirming that the optical quality of the lenticules is intact. A steeper decline in the negative control indicates that the blur has impaired the optical quality, resulting in poor transmission of information from the object at higher spatial frequencies. The MTF plot for the individual treatment condition compared to the blurred image of fresh lenticule is shown in Supplementary Figure 5.

Growth of corneal endothelium on lenticules

Human CE cells cultured on fresh SMILE lenticules for 14 days were polygonal as can be seen in Figures 6(A,B) and expressed N-cadherin (Figure 6(C)), ZO-1 (Figure 6(D)), and Na/K ATPase (Figure 6(E)), which are markers of hCE cells. As expected, there was no noticeable keratocyte nuclear staining at the end of this period. The result indicates that the keratocytes can be removed simultaneously during CE culture since the degradation of keratocyte nuclear contents did not affect the growth of the hCE cells.

SMILE lenticule as a carrier for hCE cell transplantation

Since the hCE cells were able to form a monolayer when seeded on lenticules, we wanted to assess their role as a carrier for the transplantation of the cultured cells. Cells seeded on lenticules were transplanted to edematous corneas, mounted onto artificial anterior chambers, and perfused with CE culture medium for 10 days. The average central corneal thickness was $1.44 \pm 0.241 \text{ mm}$ before perfusion (Figure 6(K)), which reduced when perfused with lenticules without cells ($p \leq 0.05$) to $1.16 \pm 0.085 \text{ mm}$ (Figure 6(K)). A further significant reduction was noted in corneas perfused with lenticules containing cells to $0.80 \pm 0.094 \text{ mm}$ ($p \leq 0.05$; Figure 6(K)) suggesting that the hCE cells on lenticules are functional. OCT images of the recipient corneas before perfusion showed the presence of increased spacing between the collagen fibers due to the fluid accumulation in the stroma (Figure 6(F)). The corneas after perfusion with lenticules without cells were thinner compared to the control, however, fluid spaces between the fibers were still noticeable (Figure 6(G)). The corneas that were perfused with lenticules containing cells had a compact and thin cornea with an orderly arrangement of collagen fibers (Figure 6(H)). The presence of the tracker dye showed that the cells remained on the lenticule after 10 days of perfusion as seen in Figure 6(J) (magnified in inset).

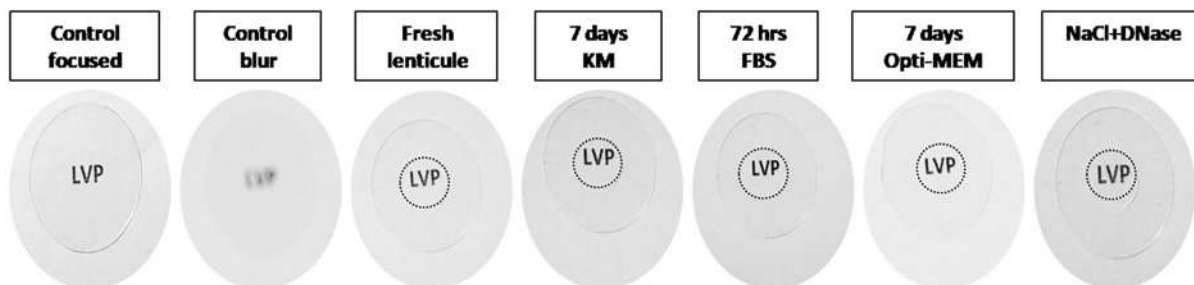
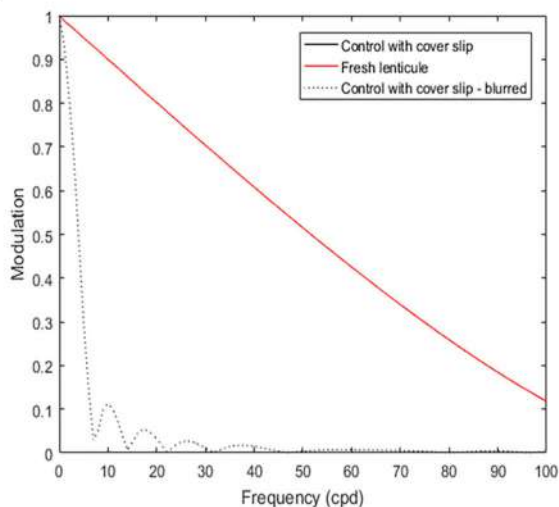
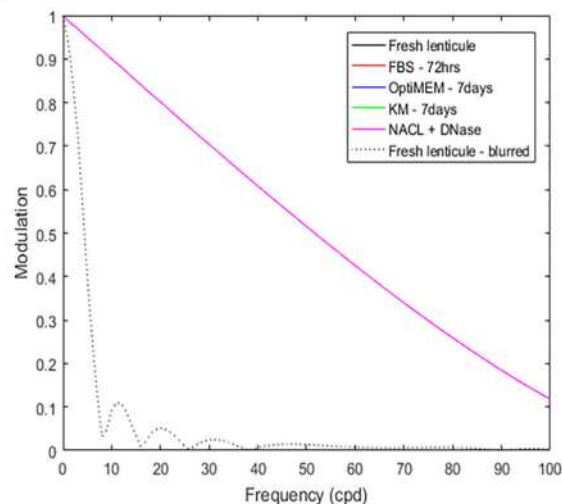
A**B****C**

Figure 5. Transparency of decellularized lenticles.

Discussion

Engineering the corneal endothelium for transplantation is an important step toward developing alternatives to cadaver donor tissues and cell injection therapy.³⁸ Several materials have been tried and tested for the same with varying degrees of success. To engineer the whole or parts of the cornea, the following criteria have to be met. The material used to support the cells should be transparent, match the refractive index of the cornea, and integrate with the native tissue in addition to being safe and compatible. The corneal stroma is the material of interest because it meets all of the above requirements. And in this study, SMILE lenticles carved out from the anterior stroma, were used for engineering the CE layer for transplantation. The lenticles were able to support the growth of the hCE cells sufficiently and mature into a functional layer of cells as evidenced by the expression of the markers namely ZO-1 and Na/K ATPase. When transplanted, the cells remained intact on the lenticles for 10 days and were able to reduce the corneal thickness significantly confirming that SMILE lenticles do provide a suitable substrate for engineering the CE layer for transplantation. Interestingly, we also found that the transplanted cells migrated onto the denuded recipient cornea (Supplementary Figure 6) indicating that the cells can repopulate the cornea following transplantation. One major limitation for clinical transplantation would be the diameter

of the lenticle, which on average is 6 mm and therefore cannot be used if a larger size of transplant is required. The smaller size would also mean that there will be little tolerance for dislocation or decentration of the lenticle following transplantation. It is also possible that the addition of the lenticles to the posterior cornea could induce a hyperopic shift in the corneal dioptric power similar to what has been reported with DSEK grafts previously.^{39–41} This is mainly due to the thickness of the lenticles which would alter the posterior radius of curvature of the cornea. The amount of hyperopic shift induced by these lenticles will have to be assessed in detail, in further studies, since the thickness of the lenticles is non-uniform (from center to periphery). However, it can be expected that the current method of decellularization would allow more allogenic lenticles to be available for implantation in the anterior cornea as inlay's for the correction of presbyopia as demonstrated by Liu *et al.*,¹³ using SMILE lenticles.

Any tissue that is used for engineering must have limited residual native DNA content to reduce the chances of rejection following transplantation. Several methods have been employed to decellularize the cornea. Since complete decellularization is difficult to achieve without compromising the tissue integrity, Crapo *et al.*³⁰ came up with the following recommendation to consider a tissue “sufficiently decellularized” and safe for transplantation: (a) the residual cellular components especially the DNA should be less than

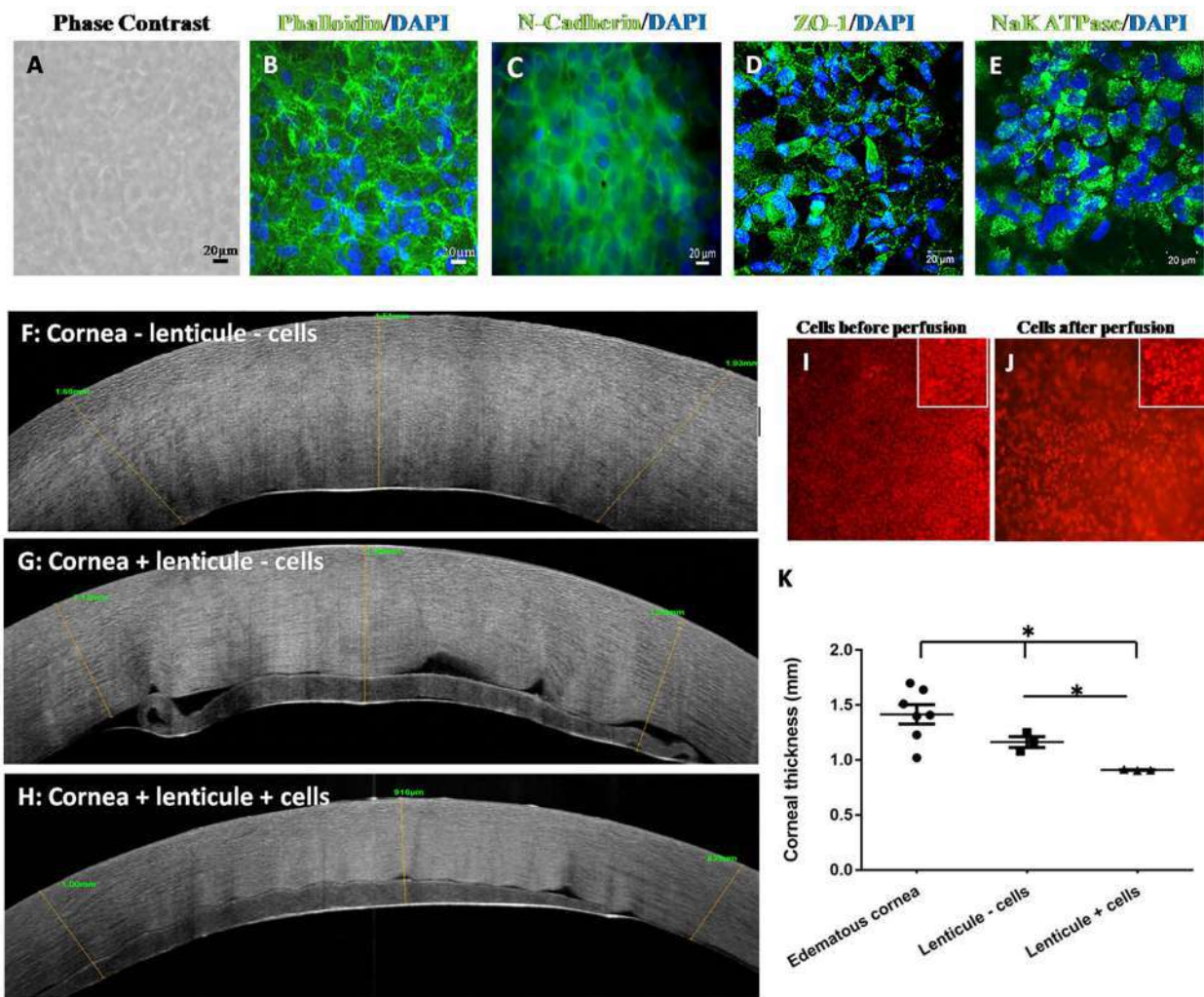


Figure 6. Functional characterization of hCE cells cultured on lenticules.

50 ng/mg of the tissue, (b) DNA fragments should be <200 bp, and (c) absence of visible nuclear material within the ECM confirmed using DAPI or H&E staining. Decellularization of SMILE lenticules with serum and Opti-MEM, as shown in this paper, comes very close to meeting the aforementioned criteria. The residual DNA was reduced to ~4 and 6.3% of the fresh lenticule when treated with Opti-MEM and serum, respectively. This is very similar to the values reported by Yam *et al.*,¹⁸ with the use of 0.1% SDS for decellularization with extensive washing and agitation.

Initial confirmation of decellularization was achieved using DAPI staining which showed that lenticules placed in Opti-MEM were comparable to lenticules decellularized using NaCl-DNase and the data conclusively point to serum as the main factor that facilitates this process. Incubation in 100% FBS decellularized the tissue in a shorter duration and was more effective in removing DNA fragments compared to NaCl-DNase. Similar use of human serum has been reported earlier in porcine corneas where the authors showed that decellularization can be achieved in 24 hrs when used along with electrophoresis.⁴² This study demonstrated apoptosis (identified using TUNEL staining) to be the mechanism that led to the removal of the keratocytes resulting in the decellularization of the corneal tissue. They

further confirmed the results *in vitro* by demonstrating the death of keratocytes within 12 hrs when cultured in the presence of serum alone. Our results also point to the fact that in addition to degradation, the degraded cell contents were cleared without the need for extensive washing when incubated in Opti-MEM or serum. This leads us to hypothesize that since keratocyte survival is not supported by 100% serum or Opti-MEM, unlike the KM, it results in their death which might trigger the endonucleases present in the serum to degrade the nuclear contents further.

Interestingly, it was noted that much of the cytoskeletal components were also removed when lenticules were placed in Opti-MEM or serum similar to NaCl-DNase treatment indicating that the incubation of lenticules in these media was able to decellularize the lenticules to more than that achieved with extensive treatment with NaCl-DNase which requires agitation and frequent change of reagents. These results taken together point to the use of Opti-MEM or serum for decellularization to be very efficient compared to the use of chemicals or enzymes that require extensive washing to remove residues to ensure their safety for human use. The use of serum will also be more clinically acceptable since many cells used for transplantation are cultured in its presence.

The incubation of lenticules in Opti-MEM or serum did not disturb the arrangement of collagen fibers within the lenticules as was evident from the PAS staining and SEM imaging. The collagen fibers remained compact and homogeneous, unlike the NaCl-DNase-treated lenticules. Quantification of the ECM proteins showed that incubation in serum did not significantly alter the expression of stromal collagens 1, 3, and 12. There was however a reduction in collagen 5 and an increase in collagen 4 in these lenticules. Interestingly, there was increased expression of collagens 3, 4, and 12 in Opti-MEM-treated lenticules. Though we are unsure of the reason for this, it could have to do with the presence of other media components in Opti-MEM in addition to serum. Staining for keratan sulfate indicated that some amount of glycoproteins is retained in lenticules treated with Opti-MEM and serum corroborating with PAS staining. Incubation of lenticules in Opti-MEM led to the swelling of the lenticules by $\sim 20\ \mu\text{m}$ when compared to fresh lenticule. This was comparable to KM and could be attributed to the swelling induced by glycoproteins within the lenticules or those present in the serum. The lack of change in the thickness of lenticules placed in serum could be due to the shorter incubation period compared to KM or Opti-MEM. On the contrary, NaCl-DNase-treated lenticules were significantly thinner compared to fresh lenticules, Opti-MEM, and serum-treated lenticules. Similar to earlier studies that have reported a significant reduction in collagen staining with the use of nucleases,¹⁸ we found a significant reduction in specifically collagens 1 and 5 in these lenticules. Taken together, it can be deduced that while NaCl-DNase is detrimental to the ECM proteins, treatment with Opti-MEM or serum preserves the architecture and ECM proteins of the stroma.

A very interesting result in this study is that the death of keratocytes and the growth of CE cells were occurring simultaneously and it is important to note that the death and degradation of the keratocyte cell components did not affect hCE growth and were not toxic to the cells. This means that prior decellularization of the lenticules is not required for culturing the cells and that both can be achieved simultaneously thus saving time, resources, and effort in the process.

Conclusion

This study provides a proof-of-concept for the use of SMILE lenticules as carriers for engineering and transplanting the corneal endothelial layer. The study also demonstrates a simple, chemical-free yet effective technique for the decellularization of the corneal SMILE lenticules. Importantly, we show that decellularization can be achieved independently or simultaneously during the process of culturing cells thus making it cost-effective, time-saving, and simple compared to other detergent or enzyme-based techniques.

Acknowledgment

Hyderabad Eye Research Foundation, LV Prasad Eye Institute, Hyderabad, Ramayamma International Eye bank, LV Prasad Eye Institute, Hyderabad.

Disclosure statement

No potential conflict of interest was reported by the author(s).

Funding

The authors thank Department of Science and Technology, Government of India for funding to CR & BB (EMR/2017/005163). The agency was not involved in the design, collection, analysis, and interpretation of the data. This work was supported by Science and Engineering Research Board.

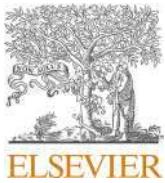
Data availability statement

The data supporting the findings of this study are available within the article and its [supplementary materials](#).

References

1. Gain P, Jullienne R, He Z, Aldossary M, Acquart S, Cognasse F, Thuret G. Global survey of corneal transplantation and eye banking. *JAMA Ophthalmol*. 2016;134(2):167–173. doi:[10.1001/jamaophthalmol.2015.4776](#).
2. Tan DT, Dart JK, Holland EJ, Kinoshita S. Corneal transplantation. *Lancet*. 2012;379(9827):1749–1761. doi:[10.1016/S0140-6736\(12\)60437-1](#).
3. Ishino Y, Sano Y, Nakamura T, Connon CJ, Rigby H, Fullwood NJ, Kinoshita S. Amniotic membrane as a carrier for cultivated human corneal endothelial cell transplantation. *Invest Ophthalmol Vis Sci*. 2004;45(3):800–806. doi:[10.1167/iops.03-0016](#).
4. Jumblatt MM, Maurice DM, Schwartz BD. A gelatin membrane substrate for the transplantation of tissue cultured cells. *Transplantation*. 1980;29(6):498–499. doi:[10.1097/00007890-198006000-00013](#).
5. Lange TM, Wood TO, McLaughlin BJ. Corneal endothelial cell transplantation using Descemet's membrane as a carrier. *J Cataract Refract Surg*. 1993;19(2):232–235. doi:[10.1016/S0886-3350\(13\)80947-9](#).
6. Mimura T, Yamagami S, Yokoo S, Usui T, Tanaka K, Hattori S, Irie S, Miyata K, Araie M, Amano S. Cultured human corneal endothelial cell transplantation with a collagen sheet in a rabbit model. *Invest Ophthalmol Vis Sci*. 2004;45(9):2992–2997. doi:[10.1167/iops.03-1174](#).
7. Mohay J, Lange TM, Soltan JB, Wood TO, McLaughlin BJ. Transplantation of corneal endothelial cells using a cell carrier device. *Cornea*. 1994;13(2):173–182. doi:[10.1097/00003226-199403000-00011](#).
8. Ramachandran C, Gupta P, Hazra S, Mandal BB. In vitro culture of human corneal endothelium on non-mulberry silk fibroin films for tissue regeneration. *Transl Vis Sci Technol*. 2020;9(4):12. doi:[10.1167/tvst.9.4.12](#).
9. Koizumi N, Sakamoto Y, Okumura N, Okahara N, Tsuchiya H, Torii R, Cooper LJ, Ban Y, Tanioka H, Kinoshita S. Cultivated corneal endothelial cell sheet transplantation in a primate model. *Invest Ophthalmol Vis Sci*. 2007;48(10):4519–4526. doi:[10.1167/iops.07-0567](#).
10. Ganesh S, Brar S, Rao PA. Cryopreservation of extracted corneal lenticules after small incision lenticule extraction for potential use in human subjects. *Cornea*. 2014;33(12):1355–1362. doi:[10.1097/ICO.0000000000000276](#).
11. Pradhan KR, Reinstein DZ, Carp GI, Archer TJ, Gobbe M, Gurung R. Femtosecond laser-assisted keyhole endokeratophakia: Correction of hyperopia by implantation of an allogeneic lenticule obtained by SMILE from a myopic donor. *J Refract Surg*. 2013;29(11):777–782. doi:[10.3928/1081597X-20131021-07](#).
12. Lim CH, Riau AK, Lwin NC, Chaurasia SS, Tan DT, Mehta JS. Lasik following small incision lenticule extraction (smile) lenticule re-implantation: A feasibility study of a novel method for

- treatment of presbyopia. PLOS One. 2013;8(12):e83046. doi:[10.1371/journal.pone.0083046](https://doi.org/10.1371/journal.pone.0083046).
13. Liu YC, Teo EPW, Ang HP, Seah XY, Lwin NC, Yam GHF, Mehta JS. Biological corneal inlay for presbyopia derived from small incision lenticule extraction (smile). Sci Rep. 2018;8(1):1831. doi:[10.1038/s41598-018-20267-7](https://doi.org/10.1038/s41598-018-20267-7).
 14. Abd Elaziz MS, Zaky AG, El SaebaySarhan AR. Stromal lenticule transplantation for management of corneal perforations; one year results. Graefes Arch Clin Exp Ophthalmol. 2017;255(6):1179–1184. doi:[10.1007/s00417-017-3645-6](https://doi.org/10.1007/s00417-017-3645-6).
 15. Bhandari V, Ganesh S, Brar S, Pandey R. Application of the smile-derived glued lenticule patch graft in microperforations and partial-thickness corneal defects. Cornea. 2016;35(3):408–412. doi:[10.1097/ICO.0000000000000741](https://doi.org/10.1097/ICO.0000000000000741).
 16. Wu F, Jin X, Xu Y, Yang Y. Treatment of corneal perforation with lenticules from small incision lenticule extraction surgery: a preliminary study of 6 patients. Cornea. 2015;34(6):658–663. doi:[10.1097/ICO.0000000000000397](https://doi.org/10.1097/ICO.0000000000000397).
 17. Yin H, Qiu P, Wu F, Zhang W, Teng W, Qin Z, Li C, Zhou J, Fang Z, Tang Q, et al. Construction of a corneal stromal equivalent with smile-derived lenticules and fibrin glue. Sci Rep. 2016;6(1):33848. doi:[10.1038/srep33848](https://doi.org/10.1038/srep33848).
 18. Yam GH, Yusoff NZ, Goh TW, Setiawan M, Lee XW, Liu YC, Mehta JS. Decellularization of human stromal refractive lenticules for corneal tissue engineering. Sci Rep. 2016;6(1):26339. doi:[10.1038/srep26339](https://doi.org/10.1038/srep26339).
 19. Brown BN, Valentin JE, Stewart-Akers AM, McCabe GP, Badylak SF. Macrophage phenotype and remodeling outcomes in response to biologic scaffolds with and without a cellular component. Biomaterials. 2009;30(8):1482–1491. doi:[10.1016/j.biomaterials.2008.11.040](https://doi.org/10.1016/j.biomaterials.2008.11.040).
 20. Xu H, Wan H, Sandor M, Qi S, Ervin F, Harper JR, Silverman RP, McQuillan DJ. Host response to human acellular dermal matrix transplantation in a primate model of abdominal wall repair. Tissue Eng Part A. 2008;14(12):2009–2019. doi:[10.1089/ten.tea.2007.0316](https://doi.org/10.1089/ten.tea.2007.0316).
 21. Vorotnikova E, McIntosh D, Dewilde A, Zhang J, Reing JE, Zhang L, Cordero K, Bedelbaeva K, Gourevitch D, Heber-Katz E, et al. Extracellular matrix-derived products modulate endothelial and progenitor cell migration and proliferation in vitro and stimulate regenerative healing *in vivo*. Matrix Biol. 2010;29(8):690–700. doi:[10.1016/j.matbio.2010.08.007](https://doi.org/10.1016/j.matbio.2010.08.007).
 22. Xu CC, Chan RW, Weinberger DG, Efun G, Pawlowski KS. A bovine acellular scaffold for vocal fold reconstruction in a rat model. J Biomed Mater Res A. 2010;92(1):18–32. doi:[10.1002/jbm.a.32279](https://doi.org/10.1002/jbm.a.32279).
 23. Allen RA, Seltz LM, Jiang H, Kasick RT, Sellaro TL, Badylak SF, Ogilvie JB. Adrenal extracellular matrix scaffolds support adrenocortical cell proliferation and function *in vitro*. Tissue Eng Part A. 2010;16(11):3363–3374. doi:[10.1089/ten.tea.2010.0005](https://doi.org/10.1089/ten.tea.2010.0005).
 24. Bayyoud T, Thaler S, Hofmann J, Maurus C, Spitzer MS, Bartz-Schmidt KU, Szurman P, Yoeuruck E. Decellularized bovine corneal posterior lamellae as carrier matrix for cultivated human corneal endothelial cells. Curr Eye Res. 2012;37(3):179–186. doi:[10.3109/02713683.2011.644382](https://doi.org/10.3109/02713683.2011.644382).
 25. Du L, Wu X. Development and characterization of a full-thickness acellular porcine cornea matrix for tissue engineering. Artif Organs. 2011;35(7):691–705. doi:[10.1111/j.1525-1594.2010.01174.x](https://doi.org/10.1111/j.1525-1594.2010.01174.x).
 26. Angunawela RI, Riau AK, Chaurasia SS, Tan DT, Mehta JS. Refractive lenticule re-implantation after myopic ReLex: a feasibility study of stromal restoration after refractive surgery in a rabbit model. Invest Ophthalmol Vis Sci. 2012;53(8):4975–4985. doi:[10.1167/iovs.12-10170](https://doi.org/10.1167/iovs.12-10170).
 27. Pang K, Du L, Wu X. A rabbit anterior cornea replacement derived from acellular porcine cornea matrix, epithelial cells and keratocytes. Biomaterials. 2010;31(28):7257–7265. doi:[10.1016/j.biomaterials.2010.05.066](https://doi.org/10.1016/j.biomaterials.2010.05.066).
 28. Ponce Marquez S, Martinez VS, McIntosh Ambrose W, Wang J, Gantxegui NG, Schein O, Elisseeff J. Decellularization of bovine corneas for tissue engineering applications. Acta Biomater. 2009;5(6):1839–1847. doi:[10.1016/j.actbio.2009.02.011](https://doi.org/10.1016/j.actbio.2009.02.011).
 29. Choi JS, Williams JK, Grevin M, Walter KA, Laber PW, Khang G, Soker S. Bioengineering endothelialized neo-corneas using donor-derived corneal endothelial cells and decellularized corneal stroma. Biomaterials. 2010;31(26):6738–6745. doi:[10.1016/j.biomaterials.2010.05.020](https://doi.org/10.1016/j.biomaterials.2010.05.020).
 30. Crapo PM, Gilbert TW, Badylak SF. An overview of tissue and whole organ decellularization processes. Biomaterials. 2011;32(12):3233–3243. doi:[10.1016/j.biomaterials.2011.01.057](https://doi.org/10.1016/j.biomaterials.2011.01.057).
 31. Gilbert TW, Sellaro TL, Badylak SF. Decellularization of tissues and organs. Biomaterials. 2006;27(19):3675–3683. doi:[10.1016/j.biomaterials.2006.02.014](https://doi.org/10.1016/j.biomaterials.2006.02.014).
 32. Shafiq MA, Gemeinhart RA, Yue BY, Djalilian AR. Decellularized human cornea for reconstructing the corneal epithelium and anterior stroma. Tissue Eng Part C Methods. 2012;18(5):340–348. doi:[10.1089/ten.TEC.2011.0072](https://doi.org/10.1089/ten.TEC.2011.0072).
 33. Gonzalez-Andrades M, de la Cruz Cardona J, Ionescu AM, Campos A, Del Mar Perez M, Alaminos M. Generation of bioengineered corneas with decellularized xenografts and human keratocytes. Invest Ophthalmol Vis Sci. 2011;52(1):215–222. doi:[10.1167/iovs.09-4773](https://doi.org/10.1167/iovs.09-4773).
 34. Wilson SL, Sidney LE, Dunphy SE, Dua HS, Hopkinson A. Corneal decellularization: A method of recycling unsuitable donor tissue for clinical translation? Curr Eye Res. 2016;41(6):769–782. doi:[10.3109/02713683.2015.1062114](https://doi.org/10.3109/02713683.2015.1062114).
 35. Yoeuruck E, Bayyoud T, Maurus C, Hofmann J, Spitzer MS, Bartz-Schmidt KU, Szurman P. Decellularization of porcine corneas and repopulation with human corneal cells for tissue-engineered xenografts. Acta Ophthalmol. 2012;90(2):e125–e131. doi:[10.1111/j.1755-3768.2011.02261.x](https://doi.org/10.1111/j.1755-3768.2011.02261.x).
 36. Joyce NC, Zhu CC. Human corneal endothelial cell proliferation: potential for use in regenerative medicine. Cornea. 2004;23(8 Suppl):S8–S19. doi:[10.1097/01.icc.0000136666.63870.18](https://doi.org/10.1097/01.icc.0000136666.63870.18).
 37. Patel SV, Bachman LA, Hann CR, Bahler CK, Fautsch MP. Human corneal endothelial cell transplantation in a human *ex vivo* model. Invest Ophthalmol Vis Sci. 2009;50(5):2123–2131. doi:[10.1167/iovs.08-2653](https://doi.org/10.1167/iovs.08-2653).
 38. Kinoshita S, Koizumi N, Ueno M, Okumura N, Imai K, Tanaka H, Yamamoto Y, Nakamura T, Inatomi T, Bush J, et al. Injection of cultured cells with a rock inhibitor for bullous keratopathy. N Engl J Med. 2018;378(11):995–1003. doi:[10.1056/NEJMoa1712770](https://doi.org/10.1056/NEJMoa1712770).
 39. Jun B, Kuo AN, Afshari NA, Carlson AN, Kim T. Refractive change after Descemet stripping automated endothelial keratoplasty surgery and its correlation with graft thickness and diameter. Cornea. 2009;28(1):19–23. doi:[10.1097/ICO.0b013e318182a4c1](https://doi.org/10.1097/ICO.0b013e318182a4c1).
 40. Holz HA, Meyer JJ, Espandar L, Tabin GC, Mifflin MD, Moshirfar M. Corneal profile analysis after Descemet stripping endothelial keratoplasty and its relationship to postoperative hyperopic shift. J Cataract Refract Surg. 2008;34(2):211–214. doi:[10.1016/j.jcrs.2007.09.030](https://doi.org/10.1016/j.jcrs.2007.09.030).
 41. Hwang RY, Gauthier DJ, Wallace D, Afshari NA. Refractive changes after Descemet stripping endothelial keratoplasty: a simplified mathematical model. Invest Ophthalmol Vis Sci. 2011;52(2):1043–1054. doi:[10.1167/iovs.10-5839](https://doi.org/10.1167/iovs.10-5839).
 42. Shao Y, Tang J, Zhou Y, Qu Y, He H, Liu Q, Tan G, Li W, Liu Z. A novel method in preparation of acellular porcine corneal stroma tissue for lamellar keratoplasty. Am J Transl Res. 2015;7(12):2612–2629.



Research article

Evidence for persistent UV-induced DNA damage and altered DNA damage response in xeroderma pigmentosa patient corneas

Jacquelyn Akepogu^{a,b}, Saumya Jakati^c, Sunita Chaurasia^d, Charanya Ramachandran^{a,*}^a Prof. Brien Holden Eye Research Centre, LV Prasad Eye Institute, Hyderabad, Telangana, India^b Manipal Academy of Higher Education, Manipal, India^c Ophthalmic Pathology Laboratory, LV Prasad Eye Institute, Hyderabad, India^d The Cornea Institute, L V Prasad Eye Institute, Hyderabad, India

ARTICLE INFO

Keywords:

Xeroderma pigmentosum

Defective DNA damage response

Cornea

Ultra violet radiation

Apoptosis

Persistent DNA damage

ABSTRACT

Xeroderma pigmentosum (XP) is a rare genetic disorder characterized by injury to the ocular surface due to exposure to ultraviolet (UV) radiation. UV-induced damage in the cells leads to the formation of cyclobutane pyrimidine dimers (CPDs) and 6-4 pyrimidine-pyrimidone photoproducts that are repaired by the NER (Nucleotide Excision Repair) pathway. Mutations in the genes coding for NER proteins, as reported in XP patients, would lead to sub-optimal damage repair resulting in clinical signs varying from photo-keratitis to cancerous lesions on the ocular surface. Here, we aimed to provide evidence for the accumulation of DNA damage and activation of DNA repair pathway proteins in the corneal cells of patients with XP. Corneal buttons of patients who underwent penetrating keratoplasty were stained to quantify DNA damage and the presence of activated DNA damage response proteins (DDR) using specific antibodies. Positive staining for pH2A.X and thymidine dimers confirmed the presence of DNA damage in the corneal cells. Positive cells were found in both control corneas and XP samples however, unlike normal tissues, positive cells were found in all cell layers of XP samples indicating that these cells were sensitive to very low levels of UV. pH2A.X-positive cells were significantly more in XP corneas ($p < 0.05$) indicating the presence of double strand breaks in these tissues. A positive expression of phosphorylated-forms of DDR proteins was noted in XP corneas (unlike controls) such as ataxia telangiectasia mutated/Rad-3 related proteins (ATM/ATR), breast cancer-1 and checkpoint kinases-1 and -2. Nuclear localization of XPA was noted in XP samples which co-localized (calculated using Pearson's correlation) with pATM (0.9 ± 0.007) and pATR (0.6 ± 0.053). The increased presence of these in the nucleus confirms that unresolved DNA damage was accumulating in these cells thereby leading to prolonged activation of the damage response proteins. An increase in pp53 and TUNEL positive cells in the XP corneas indicated cell death likely driven by the p53 pathway. For comparison, cultured normal corneal epithelial cells were exposed to UV-radiation and stained for DDR proteins at 3, 6 and 24 h after irradiation to quantify the time taken by cells with intact DDR pathway to repair damage. These cells, when exposed to UV showed nuclear translocation of DDR proteins at 3 and 6 h which reduced significantly by 24 h confirming that the damaged DNA was being actively repaired leading to cell survival. The persistent presence of the DDR proteins in XP corneas indicates that damage is being actively recognized and DNA replication is stalled, thereby causing accumulation of damaged DNA leading to cell death, which would explain the cancer incidence and cell loss reported in these patients.

1. Introduction

Xeroderma pigmentosum (XP), a rare autosomal recessive genetic disorder, is characterized by injury due to solar radiation to the exposed surfaces of the body namely, the skin and ocular surface. The reported global incidence of the disease ranges between 1 per million births to 45

per million births with higher prevalence in cultures promoting consanguineous marriages (Hirai et al., 2006; Kleijer et al., 2008; Kraemer and Slor, 1985; Messaoud et al., 2010; Soufir et al., 2010). Ocular signs vary from photo-keratitis, pterygium, corneal haze, droplet keratopathy, corneal vascularization, and dryness to cancerous lesions on the ocular surface (Brooks et al., 2013; Chaurasia et al., 2014; Goyal

* Corresponding author. Brien Holden Eye Research Centre, LV Prasad Eye Institute, Hyderabad, Telangana, 500034, India.

E-mail addresses: charanya@lvpei.org, charanya.ram@gmail.com (C. Ramachandran).<https://doi.org/10.1016/j.yexer.2024.109901>

Received 4 October 2023; Received in revised form 26 March 2024; Accepted 15 April 2024

Available online 18 April 2024

0014-4835/© 2024 Elsevier Ltd. All rights reserved.

et al., 1994; Kaliki et al., 2019; Kraemer et al., 1987; Nandyala et al., 2021; Rezaei Kanavi et al., 2008; Yam and Kwok, 2014).

The cornea absorbs different wavelengths of UV radiations ranging from 240 to 400 nm (UV-A and UV-B) (Kolozsvari et al., 2002). It is well known that the maximum UV absorption and DNA damage is encountered by the epithelial cells (Mallet and Rochette, 2013) and excessive damage can lead to photo-keratitis and transient corneal haze (Podskochoy, 2004; Podskochoy et al., 2000). These cells are capable of regeneration and the damaged cells can be replaced in addition to being repaired. Though only about 20% of the incident UV penetrates the inner layers of the cornea, cellular changes and cell death have been reported in the endothelial cells following exposure (Ringvold et al., 1982). Several studies have reported a reduction in corneal endothelial density in patients with XP compared to age matched controls indicating that low penetrance of UV in these eyes is sufficient to cause DNA damage in these cells due to defective DNA repair. Histopathological analyses of XP corneas shows thickening of the Descemet's membrane confirming the presence of damage in the deeper layers of the cornea (Aghaei et al., 2020; Chaurasia et al., 2014; Karai et al., 1984; Mohamed et al., 2016; Okubo et al., 1987).

Damage to the DNA occurs when UV is absorbed leading to the formation of cyclobutane pyrimidine dimers (CPDs) and 6-4 pyrimidine-pyrimidone photoproducts. To repair these photoproducts, the NER (Nucleotide Excision Repair) pathway, made up of several proteins, is activated. These proteins are coded for by genes labelled XPA-XPG and XPV (Costa et al., 2003). While XPA, XPC and XPE are involved in sensing the DNA damage, XPB and XPD are required for DNA strand opening around the damaged bases. Endonucleases XPG and XPF incise to release the damaged strand so that DNA can be resynthesized by the respective polymerases. XPV is not involved directly in the NER pathway but codes for DNA polymerase η (PolH) that ensures continued DNA replication downstream of damage site. Though mutations have been reported in all the genes involved in the repair pathway, XPA (25%), XPC (25%), POLH1 (21%), and XPD (15%) are the most frequently affected (Martens et al., 2021).

Normal cells actively detect and repair DNA damage, preserving DNA integrity with minimal impact. However, an accumulation of unrepaired DNA activates damage response proteins (DDR), namely ATR (Ataxia telangiectasia and Rad3-related protein) and ATM (Ataxia-Telangiectasia mutated), which halt cell cycle progression until DNA repair occurs. Direct interaction between components of the NER and DDR pathway has been demonstrated before suggesting that these pathways work together to safeguard DNA strand integrity thereby preventing mutation accumulation or propagation (Shell et al., 2009). In cases of excessive damage, cells cease repair and trigger apoptosis, with p53 playing a central role.

Previous studies have significantly contributed to understanding the clinical and histopathological changes in the corneas in XP patients (Chaurasia, 2018; Chaurasia et al., 2014; Nandyala et al., 2021; Rezaei Kanavi et al., 2008). Few studies have demonstrated UV-induced DNA damage/repair in ocular cells mainly using animal corneas or cultured cells (De Vries et al., 1998; Estil et al., 1997; Inoki et al., 2004; Mallet et al., 2016; Mallet and Rochette, 2011; Podskochoy et al., 2000; Ringvold et al., 1982). Our goal in this study was to provide evidence for the presence of persistent DNA damage in the corneal cells of XP patients.

2. Materials and methods

Study approval (LEC-BHR-P-07-21-731) was obtained from the institutional review board of L V Prasad Eye Institute, Hyderabad. Penetrating keratoplasty buttons of five patients diagnosed with XP were procured from the ocular pathology laboratory at the L. V. Prasad Eye Institute, Hyderabad. Healthy corneas ($n = 3$) that were obtained from the Ramayamma International Eye Bank, LV Prasad Eye Institute, Hyderabad, served as controls.

2.1. Immunohistochemistry

DDR antibody sampler kit (#9947) which included Phospho-ataxia telangiectasia (ATM) (Ser1981), Phospho-ataxia telangiectasia and Rad-3 related protein (ATR) (Ser428), Phospho-breast cancer 1 (BRCA1) (Ser1524), Phospho-checkpoint kinase 1 (Chk1) (Ser345), Phospho-Histone variant H2A.X (Ser139), Phospho-checkpoint kinase 2 (Chk2) (Thr68) and Phospho-p53 (Ser15) was purchased from Cell Signaling Technology, USA. Anti-thymine dimer antibody [H3] was purchased from Abcam, UK. XPA antibody was from Santa Cruz Biotechnology, Inc., USA and anti-nitrotyrosine was purchased from R&D systems, USA.

Corneal sections from paraffin embedded blocks were stained with Hematoxylin-Eosin (H&E) for identifying gross pathological changes in the tissues. The sections were deparaffinized by heating the slides at 70°C, followed by xylene washes. The sections were rehydrated using 100%, 90% and 80% ethanol and washed gently under running tap water followed by PBS wash. For antigen retrieval, the sections were treated with citrate buffer (pH 6.0) for two cycles followed by treatment with 3% hydrogen peroxide in methanol and washed with distilled water. The sections were permeabilized with 0.1% Triton X and blocked with 0.25% BSA at room temperature followed by addition of primary antibody (dilutions in Supplementary Table S1) and incubated overnight at 4°C. Sections were washed with PBS and incubated in secondary antibody (1:750 dilution) at room temperature followed by DAPI (nuclear) staining and mounted using glycerol. Imaging was done using Zeiss Airyscan LSM 880 confocal microscope.

Click-iT Plus TUNEL assay kit (Invitrogen, USA) was used to identify apoptotic cells in paraffin embedded corneal sections of healthy controls and XP patients as per the manufacturer's recommendations. Sections from normal corneas were treated with DNase 1 to induce DNA fragmentation followed by TUNEL staining which served as the positive control.

2.2. Fluorescence quantification

For thymidine dimer (TD) and pH2A.X quantification, images from three samples each of control and XP patient corneas were considered. Fluorescence intensity in the cell nucleus was calculated by subtracting the mean gray values of the background intensity from the mean value obtained from stained cells. Cells in all the layers of the cornea were included in the analysis.

2.3. Quantification of % positive cells

Images from three samples each of control and XP patient corneas were used for calculating the % positive TD and pH2A.X cells using the formula

$$\frac{\text{Number of positive cells}}{\text{Total number of cells}} \times 100$$

DAPI staining of the nucleus aided in counting the total number of cells. Cells in all the layers of the cornea were included in the analysis.

2.4. Calculation of Pearson's correlation

The co-localization of pATM and pATR with XPA was determined using ImageJ software (NIH, USA). The images were split into their respective channels (green (XPA) and red (pATM/pATR)) to analyze the degree of co-localization with the help of the JACoP plugin in ImageJ. A correlation value between 0 and 0.3 is mild, 0.3–0.6 is moderate and 0.6–1 represents good correlation.

2.5. Culture and UV irradiation of epithelial cells in vitro

Human corneal epithelial cell line (HCEC) 10.014 pRSV-T (Araki-Sasaki et al., 1995) was obtained from Dr. Sanhita Roy, LV Prasad Eye

Institute, Hyderabad. The cells were cultured in Dulbecco's modified Eagle's medium (DMEM)/F12 medium containing L-glutamine, HEPES, sodium bicarbonate, 5% FBS, epidermal growth factor (EGF) and insulin. Cells were sub-cultured using 0.25% trypsin-EDTA and passages between 20 and 40 were used in the experiments. Based on previous reports (Oh et al., 2011; Hanasoge and Ljungman, 2007), confluent epithelial cells were exposed to 10J/m² of UV-C (254 nm) radiation capable of inducing substantial DNA damage due to its high energy level. Cells were fixed at 3, 6 and 24 h after exposure for immunostaining. Once stained for the respective DDR proteins, the cells were imaged using Zeiss Airyscan LSM 880 confocal microscope. Cells that were not exposed to UV served as control. All imaging parameters were kept constant between the different time points allowing us to quantify and compare the change in the nuclear expression of a protein at the indicated time points after exposure. The fluorescence intensity in the nucleus was calculated using raw integrated density values in 30 randomly selected cells and the p values are presented as a heat map.

2.6. Statistical analyses

The fluorescence intensity, % positive cells are reported as mean \pm SD. Pearson's correlation is presented as mean+range. For significance analysis, the student unpaired *t*-test was performed using Graphpad prism software and *p* value < 0.05 was considered statistically significant.

3. Results

Corneas of five patients were included in this study. Corneal sections were stained with H&E to evaluate changes in the tissues which showed hyperplastic epithelium in 3/5 corneas, anisonucleosis and irregular or disrupted Bowman's layer (Fig. 1). The stroma in all the samples was edematous showing signs of chronic inflammation, vascularization and the presence of activated fibroblasts. In 2/5 samples, the endothelial cells were sparse. Cases 2 and 3 were not included for further analysis since the former did not have any epithelium and the latter had extensive background noise which made it difficult to distinguish positive staining from background. Listed in the table are the changes seen in each patient cornea.

3.1. Evidence for UV-induced damage

A positive expression for thymidine dimers (TD) was noted in the epithelium, stroma and the endothelium of XP and control samples (Fig. 2A a-c, a'-c'). Quantification showed that the positive cell numbers were more in XP corneas compared to control tissues though the difference was not significant (*p* = 0.12; Fig. 2B). Similarly, quantification of fluorescence intensity indicated that TD expression was higher in the XP corneas compared to control but not statistically significant (*p* = 0.285; Fig. 2C).

We stained for pH2A.X a specific marker of double strand breaks (DSB). Unlike XP samples where pH2A.X expression was found across all the layers of the cornea (Fig. 2A d'-f'); in the control corneas, pH2A.X expression was limited to a few epithelial cells and was not noted in the stromal keratocytes or corneal endothelium (Fig. 2A d-f). The positive cell numbers and fluorescence intensity were significantly higher in the XP samples (Fig. 2B) compared to control corneas (*p* = 0.04 and *p* = 0.004 respectively; Fig. 2D).

3.2. Activation of DNA damage repair pathways in patient corneas

As shown in Fig. 3, in the XP samples, localization of pATM (Fig. 3a'-c') and pATR (Fig. 3d'-f') was observed in all the cell layers of the cornea while no expression of pATM and pATR was seen in any of the corneal layers in control samples (Fig. 3 a-c, d-f). Similarly, XPA was located both in the cytoplasm and nucleus across all layers of the cornea in XP

patient samples (Fig. 3g'-i') while a negative expression of XPA was noted in the control corneas (Fig. 3g-i).

It is known that ATM and ATR are interacting partners of XPA and nuclear co-localization of XPA with pATM (Fig. 4A) and pATR (Fig. 4B) was noted in XP samples. Pearson's correlation values for XPA-pATM (*r* = 0.911 \pm 0.007) and XPA-pATR (*r* = 0.646 \pm 0.05) indicate a high level of colocalization of these proteins in the cell nuclei of XP patients (Fig. 4C). It should be noted that XPA-pATR co-localization ranged from 0 to 0.9 resulting in the means being significantly different (*p* < 0.001).

3.3. Cell cycle checkpoint activation, and DNA repair in XP corneas

A nuclear expression of checkpoint kinases - pChk1 and pChk2 can be noted in all the layers of the cornea in XP samples (Fig. 5a'-f') while their expression was restricted to the superficial epithelial cells in the control corneas (Fig. 5a-f). Similarly, positive nuclear expression of pBRCA1 was observed in all the layers of the cornea in XP samples (Fig. 5g'-i') unlike the control corneas (Fig. 5 g-i).

In addition, our data shows clear nuclear localization of pp53 in XP patient samples across all corneal layers (Fig. 6a'-c') while its localization was restricted to the superficial cells in the control epithelium (Fig. 6a). Finally, we looked for evidence of cell death using TUNEL assay and observed a strong nuclear expression of the marker in XP patient samples (Fig. 6 d'-f') which was absent in healthy controls (Fig. 6 d-f). Positive expression was also seen in control normal corneal sections that were treated with DNase 1 (Supplementary Fig. S1). Taken together, these data confirm the prolonged activation of cell cycle regulatory and repair proteins that lead to apoptosis in XP corneas. The staining performed for each of these markers in the three patient samples is provided as Supplementary Figs. S2-4.

3.4. Oxidative damage in XP corneas

An increased expression of nitrotyrosine (reactive nitrogen species marker) was noted in all the layers of the XP patient samples (Fig. 7 a'-c') compared to control (Fig. 7a-c) confirming increased oxidative damage in these tissues.

3.5. Irradiation of normal corneal epithelium and its recovery

Since cells in the normal corneas were negative for most markers despite presence of TDs signifying UV damage, we irradiated cultured corneal epithelial cells to understand the normal recovery time of cells following UV exposure. For this, irradiated cells were fixed at 3-, 6- and 24 h post-exposure and stained for the DDR markers (Panel A). Change in the nuclear expression of each marker was quantified, values plotted (Supplementary Fig. S5) and the significance value for each combination is represented as a heat map (Panel B). Unlike untreated cells (Fig. 8 A-a, B), UV exposure significantly (*p* = 0.001) increased nuclear localization of TD at 3 h which reduced at 6 and 24 h (Fig. 8A a'-a''', B). pH2A.X which was perinuclear in the untreated cells, translocated to the nucleus starting at 3 h (Fig. 8A-b', B), and peaked at 6 h. This was significantly higher when compared to control (Fig. 8b) and reduced by 24 h (*p* = 0.001; Fig. 8A-b''', B). Similarly, pATM which was cytoplasmic in the untreated cells (Fig. 8A-c) rapidly translocated to the nucleus by 3 h (*p* = 0.001; Fig. 8A-c', B) after exposure and returned to the cytoplasm at 6-24 h with few cells showing spots of nuclear staining (Fig. 8A-c''-c''', B). Contrary to pATM, a nuclear localization of pATR (Fig. 8A-d, B) and XPA (Fig. 8A e-e''', B) was observed in untreated cells which progressively became cytoplasmic from 6 to 24 h. A marked increase in the nuclear expression of the checkpoint kinases-pChk1, pChk2 was noted by 3 h (*p* = 0.01 and *p* = 0.05 respectively) in the irradiated cells which reduced by 24 h (Fig. 8Af-f'''& g-g''', B respectively). In the untreated cells, pChk1 was localized to the cytoplasm (Fig. 8A-f) unlike pChk2 which was faintly expressed in the cell nucleus of few cells (Fig. 8A-g). Like the check point kinases, a significant increase in the expression of

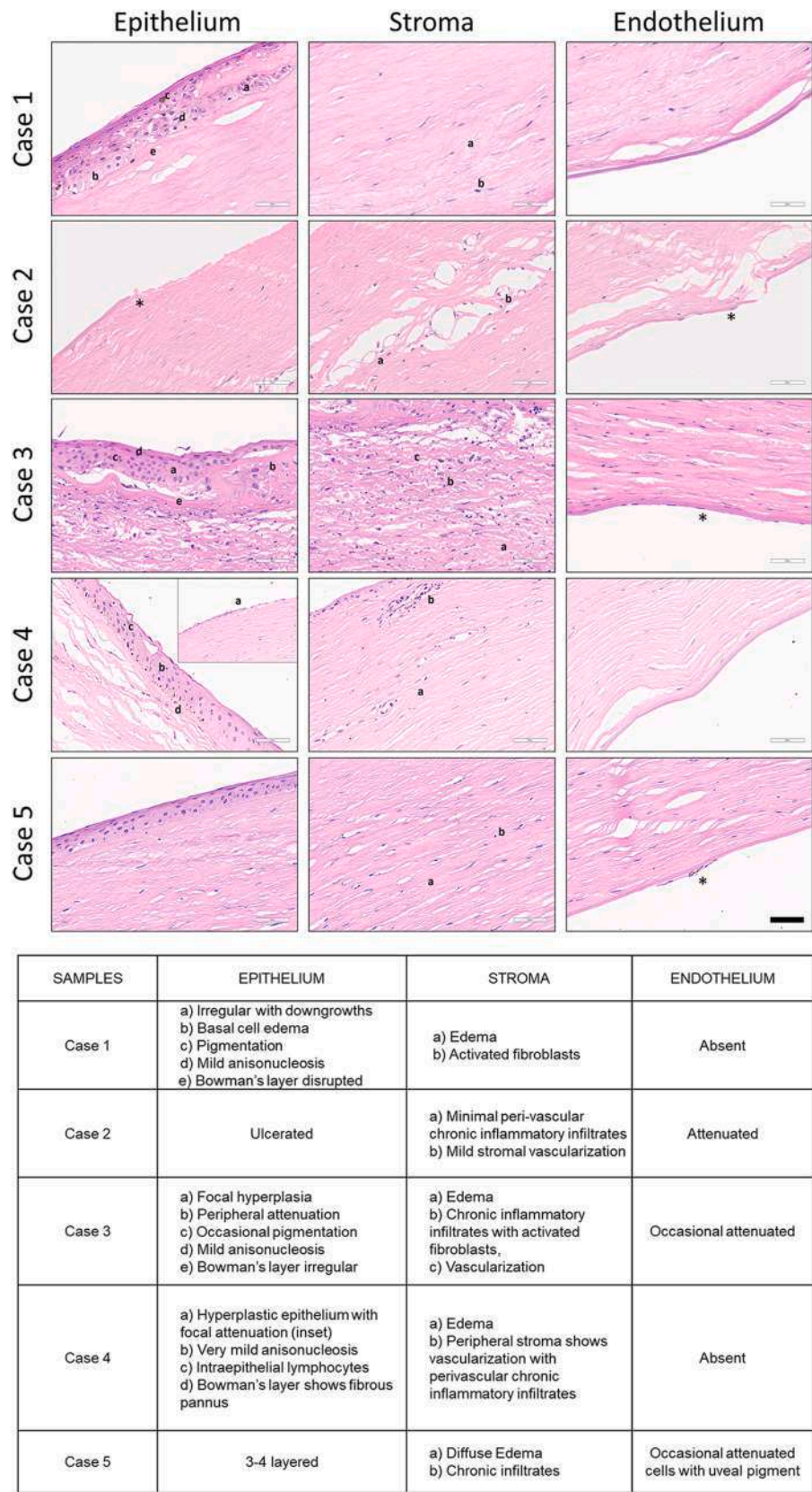


Fig. 1. Gross pathological changes in XP tissues. Hematoxylin and eosin staining was performed on 5 patient samples and the detailed findings are given in the table. The histological findings listed in the table for each patient sample are marked using alphabets and asterisk that corresponds to the labeling in the figure. Images taken at 40x (Scalebar – 60 μm).

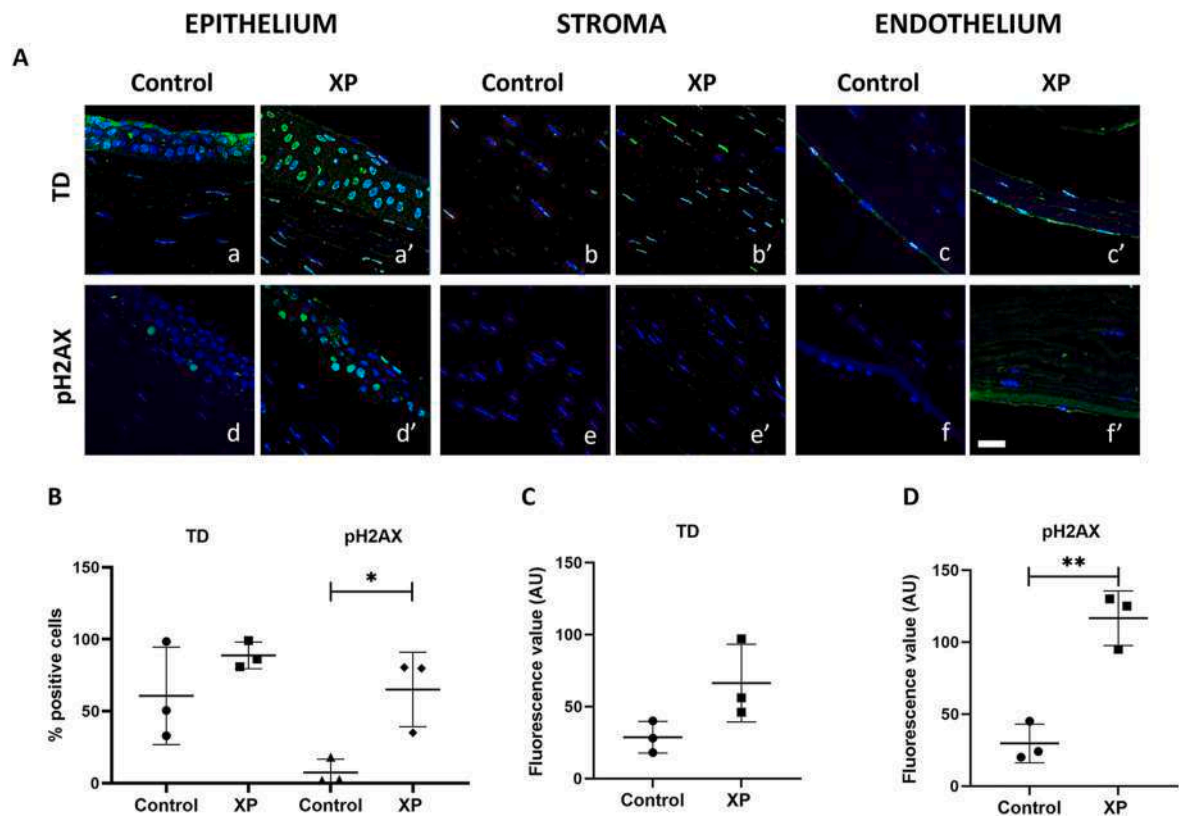


Fig. 2. DNA damage markers in XP patient samples. Panel A shows positive expression for thymidine dimers (TD) across all the corneal layers in both the control (a–c) and the XP samples (a'–c'). Expression of pH2A.X was found in few of the epithelial cells in the control samples compared to the XP samples where a positive expression was observed in all the cell layers (d'–f'). The % positive cells for TD and pH2A.X are shown in panel B. Quantification of fluorescence intensity for TD and H2A.X are shown in panels C and D, respectively. The values are plotted as mean \pm SD; scale bar – 20 μ m; * p < 0.05; ** p < 0.01.

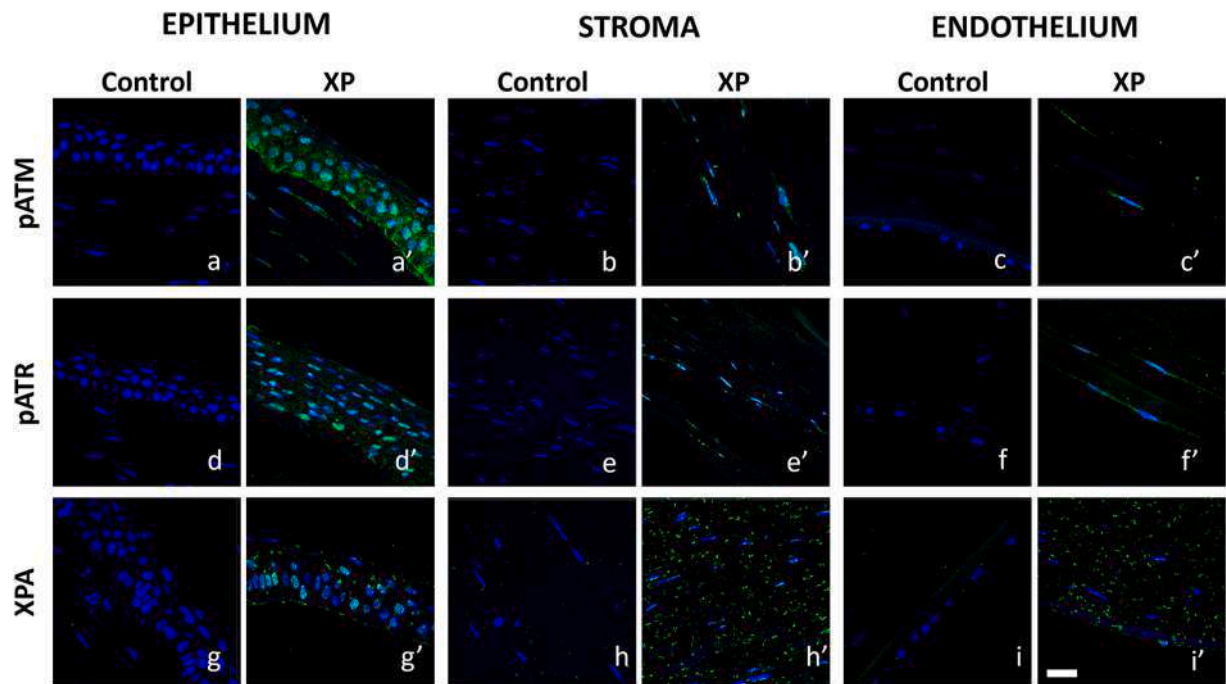


Fig. 3. Increased expression of DDR and NER proteins in XP samples. A positive nuclear expression of pATM (a'–c'), pATR (d'–f') and XPA (g'–i') was noted in all the cell layers – epithelium, stroma and endothelium in XP samples. No expression was observed in control samples for all the markers (a–i). Scalebar – 20 μ m.

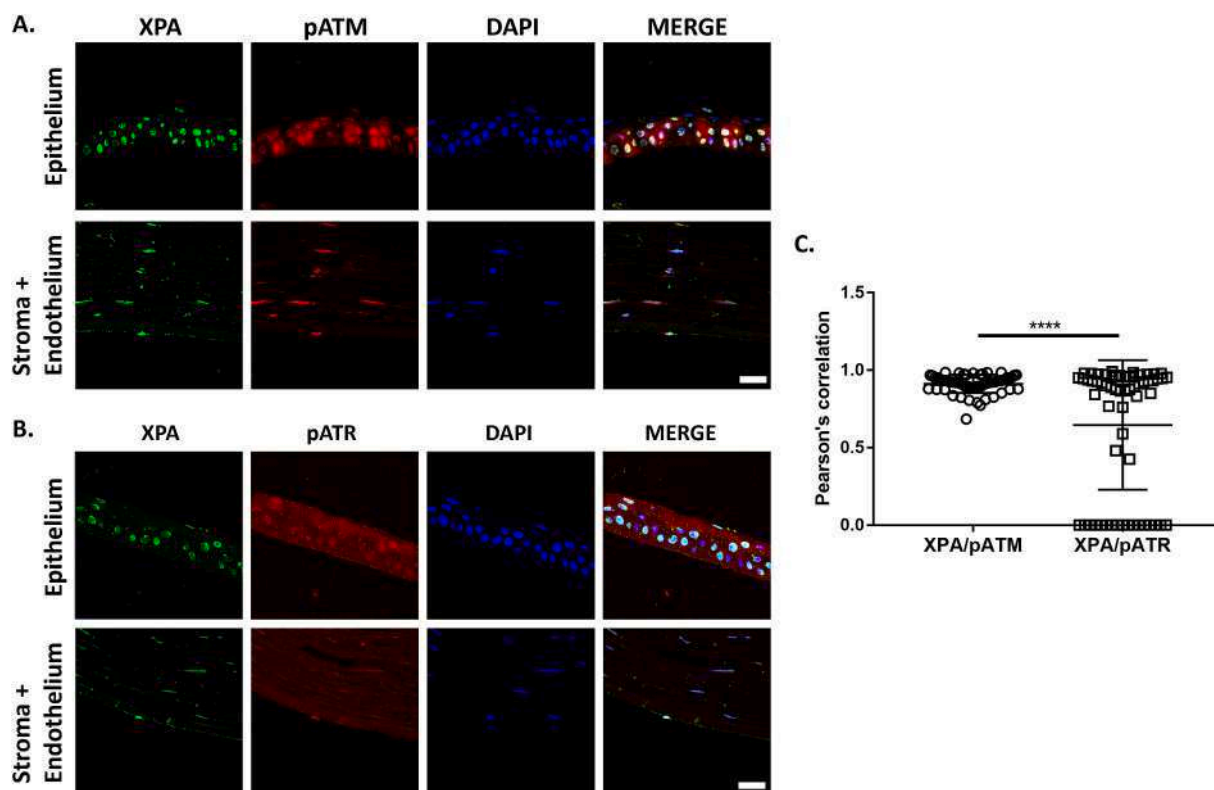


Fig. 4. Colocalization of p-ATM/p-ATR with XPA. Dual staining for pATM/pATR and XPA showed colocalization of the proteins (panels A and B). Quantification of Pearson's correlation showed that XPA strongly colocalized with pATM while its colocalization with pATR was highly variable in XP patient samples (panel C). The values are plotted as mean+range. Note: pATM/pATR-red; XPA-green; Dapi-blue; Scalebar – 20 μ m; **** = $p < 0.0001$. (For interpretation of the references to colour in this figure legend, the reader is referred to the Web version of this article.)

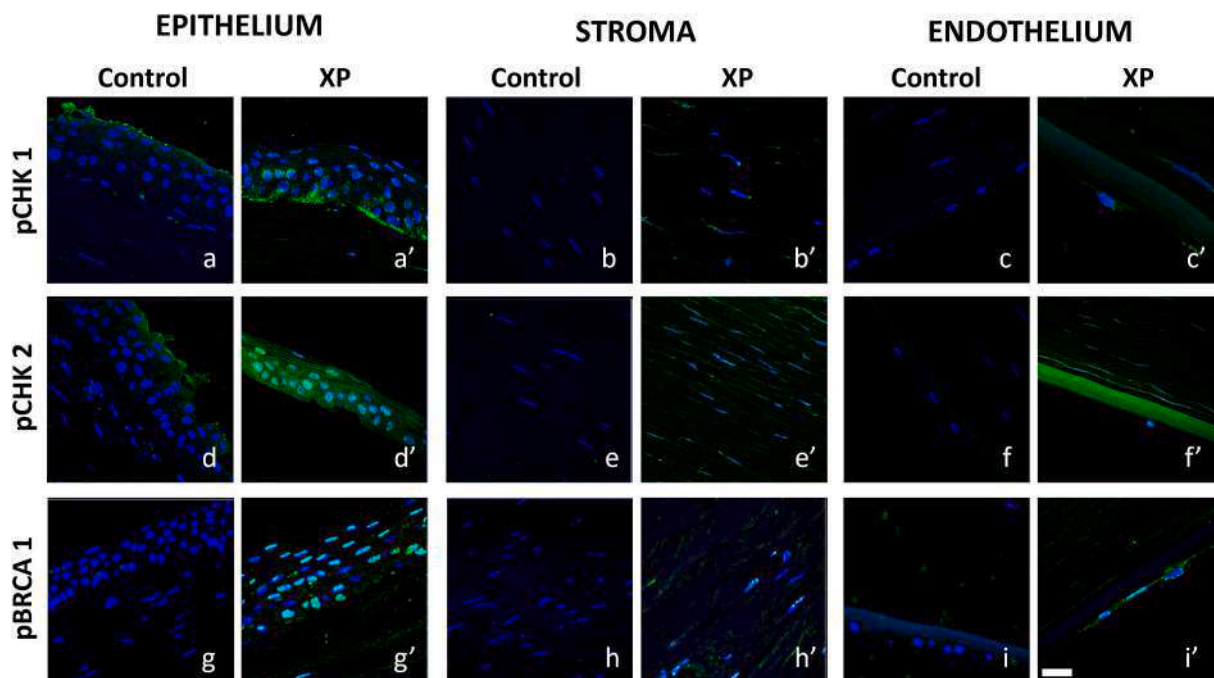


Fig. 5. Activation of checkpoint kinases. Immunostaining for pChk1 and pChk2 revealed a positive expression in XP patient samples. The phosphorylated proteins were localized to the nucleus and were observed across all the layers of the XP samples (a'-f'). A faint expression in the superficial epithelial layer was noted with no expression in the stroma and the endothelium of control corneas (a-f). Distinct nuclear expression of pBRCA1 was noted in the XP patient samples (g'-i') with no expression in the control corneas (g-i). Scalebar – 20 μ m.

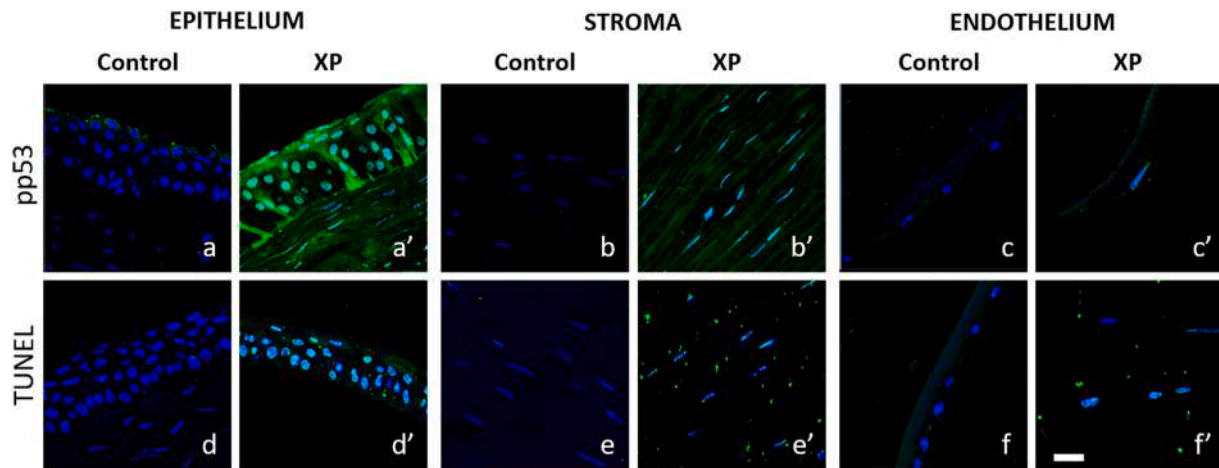


Fig. 6. Evidence for apoptosis. Staining for pp53 (a'–c') and TUNEL (d'–f') indicates the activation of apoptosis in XP patient samples. Superficial epithelial cells were positive for pp53 (6a) while no TUNEL positive cells were noted in the control samples (d–f). Scalebar – 20 μ m.

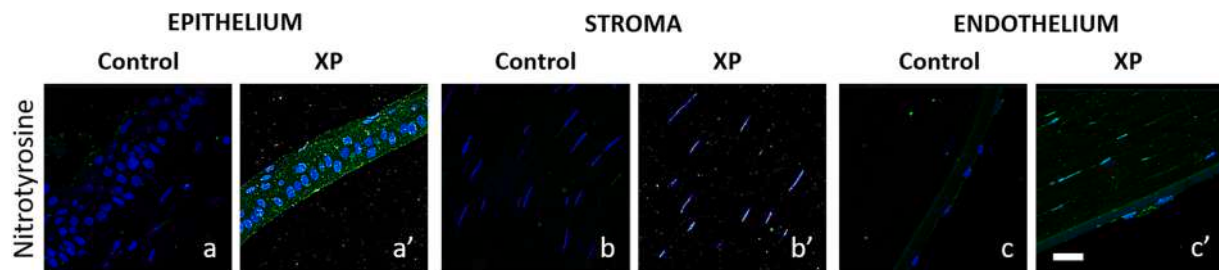


Fig. 7. Evidence for oxidative stress. Staining for Nitrotyrosine (a'–c') indicates the presence of oxidative damage in XP patient samples while mild expression for the marker was found in control corneas (a–c). Scalebar – 20 μ m.

pBRCA1 and pp53 at 3 and 6 h was noted which reduced by 24 h ($p = 0.001$) (Fig. 8A–h–h'', i–i'', B). pBRCA1 expression was faint in the untreated cells (Fig. 8A–h) and very few cells expressed pp53 (Fig. 8A–i).

Together, this data confirms activation and nuclear localization of the DDR proteins in response to UV irradiation at the early time point of 3–6 h which reduces considerably by 24 h indicating that normal cells repair the damaged DNA and recover. Live-dead assay was performed to confirm the viability of the cells post-irradiation as shown in Supplementary Fig. S6.

4. Discussion

This study shows presence of DNA damage throughout the cornea in XP patients, concomitant with the activation of key DDR pathway components that localized to damage sites. Their absence in control corneas confirms persistent DNA damage due to defective NER repair, providing evidence for cell loss that has been reported clinically. Notably, even limited UV exposure can harm the endothelial cells. Although UV is the primary insult, presence of chronic inflammation and oxidative stress suggest many contributing factors to the disease phenotype.

4.1. DNA damage repair

It has been shown that keratinocytes exposed to UV for a day in sun can accrue close to 10^5 photoproducts namely CPDs and 6-4 PPs (Hoeijmakers, 2009). These lesions are cleared via NER that has two sub pathways: Transcription Coupled-NER and Global Genome-NER. TC-NER removes lesions from transcribed strands of active genes, while GG-NER is transcription independent. Both pathways use common

elements to identify DNA damage, including TFIIH, XPA, and RPA. XPA stabilizes the unwound DNA bubble, allowing XPG and XPF to cleave the damaged site. RPA recruits ATR to the site of damage and activates its downstream signaling, which prevents the progression of cell cycle until repair is complete. If damage identification or repair synthesis is impaired, it can result in apoptosis.

Staining for TD confirmed the presence of UV damage in both control and the patient samples with more damage localized to the epithelial cells. This finding is similar to the report by Mallet et al. (Mallet and Rochette, 2013) which showed that while exposure to UV-A, B and -C induced formation of CPDs in the epithelial cells, which is expected since this layer acts as a shield protecting the eye from radiation (Podskochy, 2004), it was only UVA that could penetrate deeper into the corneal layers to induce CPD formation in posterior stroma and endothelium. XP corneas showed significantly higher TD fluorescence in all three cell layers, suggesting suboptimal clearance, further confirmed by the absence of TD in untreated cultured cells. TD accumulated in cell nuclei 3 h after UV exposure, dispersing at 6 h and 24 h from the nucleus, indicating rapid repair. TC-NER primarily handles early CPD repair (68% on transcribed strands), while GG-NER repairs slowly, explaining the residual staining at 24 h in these cells.

As previously mentioned, RPA recruits ATR, the primary PI3K kinase responding to UV radiation, to damage sites with ATRIP's (ATR interacting protein) assistance. ATR's primary role is to halt cell cycle progression by activating Chk1. In XP tissues, there was increased nuclear pATR expression with a concomitant increase in the nuclear expression of pChk1 compared to control confirming the recruitment of these proteins to the sites of DNA damage potentially stalling cell cycle progression. A similar result was obtained with cultured cells for pChk1 which translocated to the nucleus after UV exposure and reduced to control levels by 24 h. Interestingly, pATR levels were significantly

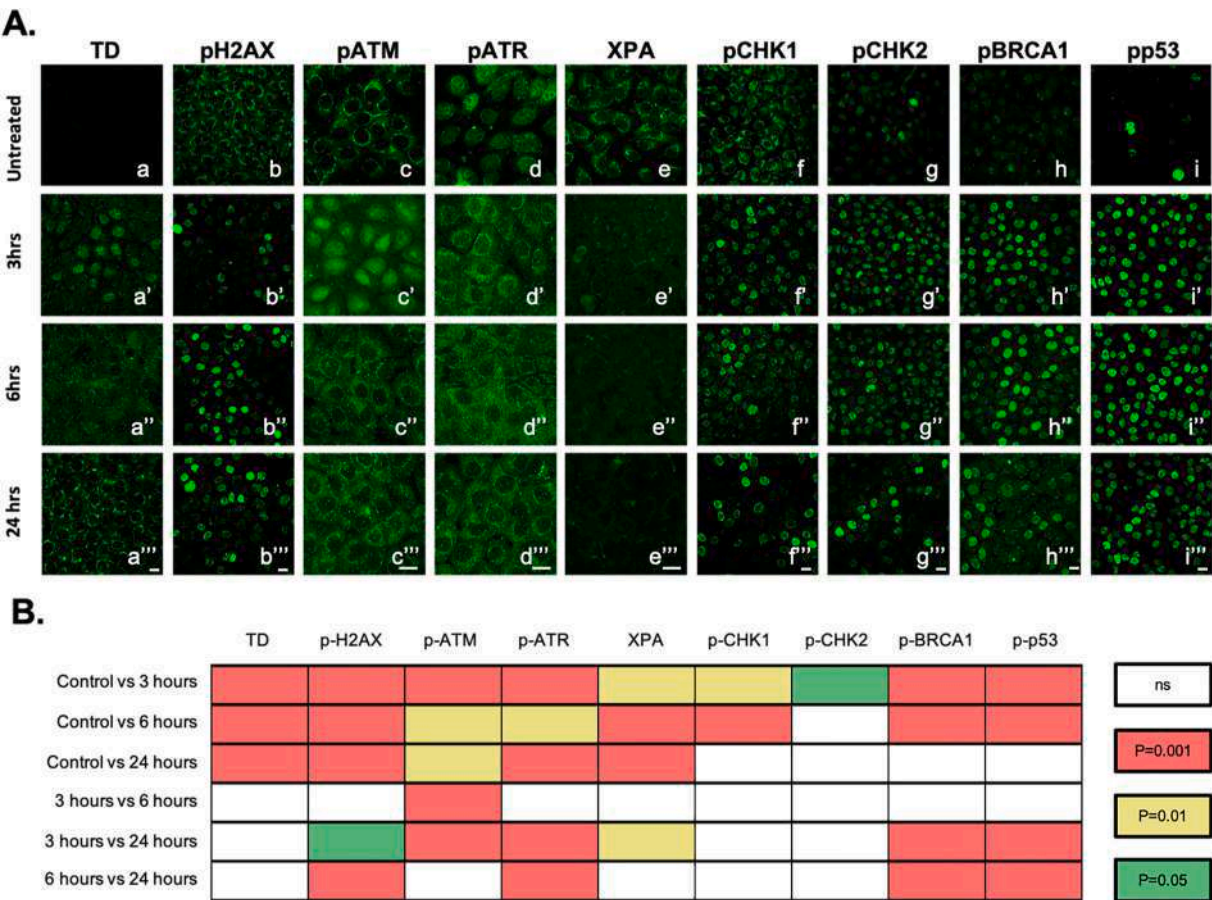


Fig. 8. UV-induced DNA damage repair in normal cells. In panel A, a marked increase in the nuclear translocation and activation was observed for most markers at 3 (a'-i') or 6 h (a''-i'') after UV-radiation. XPA (e-e'') and pATR (d-d'') showed a decrease at 3 and 6 h compared to control. The number of positive cells and the fluorescence intensity at the nucleus reduced by 24 h showing successful repair and recovery of cells (a'''-i'''). Panel B is a heat map of p values across all markers compared at the different time points. Scalebar- 20 μ m (TD, pH2A.X, pChk1, pChk2, pBRCA1, pp53) and 50 μ m (pATM, pATR, XPA).

higher in untreated cells compared to post-exposure time points. It is possible that UV exposure accelerated existing DNA damage (part of normal cell division) repair by concentrating repair proteins at the damage sites.

4.2. Double strand break repair

While UV exposure doesn't directly create DSBs, they form during replication of unrepaired DNA damage. Unlike control, XP tissues showed widespread staining for pH2A.X across cell layers. These tissues had more pH2A.X-positive cells and the staining intensity was significantly more confirming increased DSB presence. That H2A.X is a target of ATM was evident in the cultured cells where pATM's nuclear localization peaked at 3 h and normalized by 6 h while pH2A.X expression peaked at 6 h, indicating a temporal delay in its activation confirming that it acts downstream of ATM(Kurose et al., 2005). ATM is generally inactive in undamaged cells and is recruited to the sites of DSB by the Mre11-Rad50-Nbs-1 (MRN) protein complex. This is obvious in the untreated cell line (Fig. 8A) where the protein is localized to the cytoplasm until exposure to UV which leads to its nuclear translocation. Once activated, ATM phosphorylates its other downstream effectors such as BRCA1 and Chk2 (Kurose et al., 2005). pATM activation of Chk2, would result in G1/S or G2/M checkpoint activation while the activation of BRCA1, either directly or via Chk2, would promote DSB repair through homologous recombination. The strong expression of pATM and activation of BRCA1 suggest that there might be some resolution of DSBs through recombination and end joining. This in addition to the presence of the inherent tolerance mechanism called translesion

synthesis which allows the cells to bypass the replication block and continue DNA synthesis downstream of the damage site could explain the survival of the corneal cells for a decade or more despite damage in these patients before they require surgery.

The ATR-Chk1 and ATM-Chk2 pathways function to stall replication by inhibiting CDC25 phosphatases resulting in their degradation. These pathways ultimately activate p53 the tumour suppressor protein which acts as the aggregator of many signalling pathways and defines whether the cell responds to stress by inducing senescence, apoptosis, cell-cycle arrest, or repair. Research indicates that p53 responds to radiation damage in pulses. Fewer pulses promote cell survival while sustained pulses lead to cell death (Zhang et al., 2009). pp53 was strongly expressed in all the corneal layers of the XP samples (Fig. 6) similar to the cell line at 3- and 6-h post-irradiation (Fig. 8). Its expression in the cell line decreased significantly by 24 h indicating successful repair promoting cell survival which was confirmed by the live-dead assay. Prolonged activation of p53 taken together with TUNEL positivity indicates cell death in the XP samples, consistent with clinical evidence.

4.3. XPA: the common denominator

While DNA damage can be recognized independently by both the NER pathway and the checkpoint machinery, a study has pointed to XPA as the common factor between these pathways in driving DNA repair (Wu et al., 2007). We specifically targeted XPA since this protein is central to both GG-NER and TC-NER, its recruitment to the DNA damage site is critical for subsequent repair, it associates directly with ATR, and nearly 25% of XP phenotype is attributed to mutations in its gene

(Borszekova Pulzova et al., 2020). In patient samples, XPA localized to the nucleus, confirming its recruitment to DNA damage sites. In cultured cells, curiously, XPA staining intensity in treated cell nuclei decreased significantly from 3 to 24 h compared to untreated cells. XPA is one of the first proteins to recognize and respond to damage by recruiting NER and DDR proteins sequentially and this happens as early as 30 min post irradiation (Volker et al., 2001). XPA activation and nuclear translocation might have occurred earlier than the 3 h time point in this study, warranting further detailed research on its role in the cell's response to UV damage. In a study by Wu et al. (2007) the authors showed that there was a direct interaction between XPA and ATR and the elimination of ATR (using inhibitors or siRNA) prevented the phosphorylation of XPA. Though ATR is the main activator of XPA in response to UV radiation, it can be activated by ATM and DNA-PK. The colocalization of XPA and pATR was variable when compared to pATM, possibly due to conversion of unresolved SSBs to DSBs. This notion is supported by the strong expression of pH2A.X in these cells suggesting that ATM activation and DSB repair take prominence over ATR pathway in cells with unresolved damage. These results clearly demonstrate a crosstalk between NER and DDR pathways in UV-damaged cells.

4.4. Role of oxidative stress and inflammation

Apart from UV, oxidative stress and inflammation can cause additional DNA damage (Hirota et al., 2005; Kulms et al., 2002; Murata and Kawanishi, 2004). Evidence for chronic inflammation was present in every XP sample reported in this study (Fig. 1). Similarly, in the XP sample tested (Fig. 7) there was increased expression of nitrotyrosine compared to the control confirming presence of oxidative stress in the tissue. Similar findings have been reported in patients with congenital hereditary endothelial dystrophy contributing to endothelial dysfunction and eventual death (Guha et al., 2017). Earlier studies have demonstrated that patients with mutations in XPA have neurological symptoms that develop over several decades despite the brain being protected from UV. This is thought to be due to the accumulation of lesions mainly cyclopurines (induced by ROS) that accumulate in the non-dividing neuronal cells and can be repaired by NER resulting eventually in their death (Brooks, 2007). We surmise that a similar mechanism may accelerate corneal endothelial loss in XP patients in addition to UV.

5. Conclusion

Kinase proteins are typically activated by DNA damage and return to baseline levels once the damage is repaired. However, in cells with unrepaired DNA damage, these kinases remain activated promoting partial repair and eventually cell death or tumors in XP patients. Our study has a few limitations, namely small sample size and the absence of information on the NER mutation background in these patients. Though we tried to include more samples in the study and screened many patient samples, we were limited by the quality of the tissue which either had poor epithelial or endothelial cell numbers and therefore we included only three samples in this study. The second limitation is something we aim to address in a future study by screening the patients for mutations and then correlate the findings at the tissue level with the mutation background. Nevertheless, the results of this study show significant accumulation of DNA damage in these cells and their adverse effect on cell survival.

Funding

This research did not receive any specific grant from funding agencies in the public, commercial, or not-for-profit sectors.

CRediT authorship contribution statement

Jacquelyn Akepogu: Writing – review & editing, Writing – original draft, Visualization, Validation, Methodology, Investigation, Formal analysis, Data curation. **Saumya Jakati:** Writing – review & editing, Visualization, Investigation, Formal analysis. **Sunita Chaurasia:** Writing – review & editing, Writing – original draft, Conceptualization. **Charanya Ramachandran:** Writing – review & editing, Writing – original draft, Validation, Supervision, Resources, Project administration, Methodology, Investigation, Funding acquisition, Data curation, Conceptualization.

Declaration of competing interest

None of the authors have any financial or non-financial conflicts of interest.

Data availability

Data will be made available on request.

Acknowledgements

We thank Dr. Ponnari Gotipatti, LV Prasad Eye Institute for her invaluable suggestions for improving the quality of the manuscript.

Appendix A. Supplementary data

Supplementary data to this article can be found online at <https://doi.org/10.1016/j.exer.2024.109901>.

References

- Aghaei, H., Es'haghi, A., Pourmatin, R., Mohammadi, A., Kashkouli, M.B., 2020. Corneal endothelial assessment in xeroderma pigmentosum: a case-control study. *Int. Ophthalmol.* 40, 2179–2183.
- Araki-Sasaki, K., Ohashi, Y., Sasabe, T., Hayashi, K., Watanabe, H., Tano, Y., Handa, H., 1995. An SV40-immortalized human corneal epithelial cell line and its characterization. *Invest. Ophthalmol. Vis. Sci.* 36, 614–621.
- Borszekova Pulzova, L., Ward, T.A., Chovanec, M., 2020. XPA: DNA repair protein of significant clinical importance. *Int. J. Mol. Sci.* 21.
- Brooks, B.P., Thompson, A.H., Bishop, R.J., Clayton, J.A., Chan, C.C., Tsilou, E.T., Zein, W.M., Tamura, D., Khan, S.G., Ueda, T., Boyle, J., Oh, K.S., Imoto, K., Inui, H., Moriwaki, S., Emmert, S., Iliff, N.T., Bradford, P., Digiovanna, J.J., Kraemer, K.H., 2013. Ocular manifestations of xeroderma pigmentosum: long-term follow-up highlights the role of DNA repair in protection from sun damage. *Ophthalmology* 120, 1324–1336.
- Brooks, P.J., 2007. The case for 8,5'-cyclopurine-2'-deoxynucleosides as endogenous DNA lesions that cause neurodegeneration in xeroderma pigmentosum. *Neuroscience* 145, 1407–1417.
- Chaurasia, S., 2018. Corneal edema in xeroderma pigmentosa. *Indian J. Ophthalmol.* 66, 1622.
- Chaurasia, S., Mulay, K., Ramappa, M., Sangwan, V., Murthy, S., Nair, R., Vemuganti, G., 2014. Corneal changes in xeroderma pigmentosum: a clinicopathologic report. *Am. J. Ophthalmol.* 157, 495–500 e492.
- Costa, R.M., Chigancas, V., Galhardo Rda, S., Carvalho, H., Menck, C.F., 2003. The eukaryotic nucleotide excision repair pathway. *Biochimie* 85, 1083–1099.
- De Vries, A., Gorgels, T.G., Berg, R.J., Jansen, G.H., Van Steeg, H., 1998. Ultraviolet-B induced hyperplasia and squamous cell carcinomas in the cornea of XPA-deficient mice. *Exp. Eye Res.* 67, 53–59.
- Estil, S., Olsen, W.M., Huitfeldt, H.S., Haaskjold, E., 1997. UVB-induced formation of (6-4) photoproducts in the rat corneal epithelium. *Acta Ophthalmol. Scand.* 75, 120–123.
- Goyal, J.L., Rao, V.A., Srinivasan, R., Agrawal, K., 1994. Oculocutaneous manifestations in xeroderma pigmentosa. *Br. J. Ophthalmol.* 78, 295–297.
- Guha, S., Chaurasia, S., Ramachandran, C., Roy, S., 2017. SLC4A11 depletion impairs NRF2 mediated antioxidant signaling and increases reactive oxygen species in human corneal endothelial cells during oxidative stress. *Sci. Rep.* 7, 4074.
- Hanasoge, S., Ljungman, M., 2007. H2AX phosphorylation after UV irradiation is triggered by DNA repair intermediates and is mediated by the ATR kinase. *Carcinogenesis* 28, 2298–2304.
- Hirai, Y., Kodama, Y., Moriwaki, S., Noda, A., Cullings, H.M., Macphee, D.G., Kodama, K., Mabuchi, K., Kraemer, K.H., Land, C.E., Nakamura, N., 2006. Heterozygous individuals bearing a founder mutation in the XPA DNA repair gene comprise nearly 1% of the Japanese population. *Mutat. Res.* 601, 171–178.

- Hirota, A., Kawachi, Y., Itoh, K., Nakamura, Y., Xu, X., Banno, T., Takahashi, T., Yamamoto, M., Otsuka, F., 2005. Ultraviolet A irradiation induces NF-E2-related factor 2 activation in dermal fibroblasts: protective role in UVA-induced apoptosis. *J. Invest. Dermatol.* 124, 825–832.
- Hoeijmakers, J.H., 2009. DNA damage, aging, and cancer. *N. Engl. J. Med.* 361, 1475–1485.
- Inoki, T., Endo, H., Inoki, Y., Hamamoto, T., Tsuru, T., Mori, T., Miyata, K., Amano, S., Yamagami, S., 2004. Damaged DNA-binding protein 2 accelerates UV-damaged DNA repair in human corneal endothelium. *Exp. Eye Res.* 79, 367–376.
- Kaliki, S., Jajapuram, S.D., Maniar, A., Mishra, D.K., 2019. Ocular and periocular tumors in xeroderma pigmentosum: a study of 120 asian Indian patients. *Am. J. Ophthalmol.* 198, 146–153.
- Karai, I., Matsumura, S., Takise, S., Horiguchi, S., Matsuda, M., 1984. Morphological change in the corneal endothelium due to ultraviolet radiation in welders. *Br. J. Ophthalmol.* 68, 544–548.
- Kleijer, W.J., Laugel, V., Berneburg, M., Nardo, T., Fawcett, H., Gratchev, A., Jaspers, N. G., Sarasin, A., Stefanini, M., Lehmann, A.R., 2008. Incidence of DNA repair deficiency disorders in western Europe: xeroderma pigmentosum, Cockayne syndrome and trichothiodystrophy. *DNA Repair* 7, 744–750.
- Kolozsvári, L., Nogradi, A., Hopp, B., Bor, Z., 2002. UV absorbance of the human cornea in the 240- to 400-nm range. *Invest. Ophthalmol. Vis. Sci.* 43, 2165–2168.
- Kraemer, K.H., Lee, M.M., Scotto, J., 1987. Xeroderma pigmentosum. Cutaneous, ocular, and neurologic abnormalities in 830 published cases. *Arch. Dermatol.* 123, 241–250.
- Kraemer, K.H., Slor, H., 1985. Xeroderma pigmentosum. *Clin. Dermatol.* 3, 33–69.
- Kulms, D., Zeise, E., Poppelmann, B., Schwarz, T., 2002. DNA damage, death receptor activation and reactive oxygen species contribute to ultraviolet radiation-induced apoptosis in an essential and independent way. *Oncogene* 21, 5844–5851.
- Kurose, A., Tanaka, T., Huang, X., Halicka, H.D., Traganos, F., Dai, W., Darzynkiewicz, Z., 2005. Assessment of ATM phosphorylation on Ser-1981 induced by DNA topoisomerase I and II inhibitors in relation to Ser-139-histone H2AX phosphorylation, cell cycle phase, and apoptosis. *Cytometry* 68, 1–9.
- Mallet, J.D., Dorr, M.M., Drigeard Desgarnier, M.C., Bastien, N., Gendron, S.P., Rochette, P.J., 2016. Faster DNA repair of ultraviolet-induced cyclobutane pyrimidine dimers and lower sensitivity to apoptosis in human corneal epithelial cells than in epidermal keratinocytes. *PLoS One* 11, e0162212.
- Mallet, J.D., Rochette, P.J., 2011. Ultraviolet light-induced cyclobutane pyrimidine dimers in rabbit eyes. *Photochem. Photobiol.* 87, 1363–1368.
- Mallet, J.D., Rochette, P.J., 2013. Wavelength-dependent ultraviolet induction of cyclobutane pyrimidine dimers in the human cornea. *Photochem. Photobiol. Sci.* 12, 1310–1318.
- Martens, M.C., Emmert, S., Boeckmann, L., 2021. Xeroderma pigmentosum: gene variants and splice variants. *Genes* 12.
- Messaoud, O., Ben Rekaya, M., Cherif, W., Talmoudi, F., Boussen, H., Mokhtar, I., Boubaker, S., Amouri, A., Abdelhak, S., Zghal, M., 2010. Genetic homogeneity of mutational spectrum of group-A xeroderma pigmentosum in Tunisian patients. *Int. J. Dermatol.* 49, 544–548.
- Mohamed, A., Peguda, R., Ramappa, M., Ali, M.J., Chaurasia, S., 2016. Corneal endothelium in xeroderma pigmentosum: clinical specular microscopy study. *Br. J. Ophthalmol.* 100, 750–753.
- Murata, M., Kawanishi, S., 2004. Oxidative DNA damage induced by nitrotyrosine, a biomarker of inflammation. *Biochem. Biophys. Res. Commun.* 316, 123–128.
- Nandyala, S., Mohamed, A., Chaurasia, S., Kaliki, S., Ramappa, M., Vemuganti, G.K., 2021. Ocular features in a large cohort of Indians with xeroderma pigmentosum. *Cornea* 40, 571–577.
- Oh, K.S., Bustin, M., Mazur, S.J., Appella, E., Kraemer, K.H., 2011. UV-induced histone H2AX phosphorylation and DNA damage related proteins accumulate and persist in nucleotide excision repair-deficient XP-B cells. *DNA Repair* 10, 5–15.
- Okubo, K., Nakamura, M., Nomura, K., Kawakami, J., Ichihashi, M., 1987. The corneal endothelium in xeroderma pigmentosum. *Ophthalmologica* 195, 178–182.
- Podskochy, A., 2004. Protective role of corneal epithelium against ultraviolet radiation damage. *Acta Ophthalmol. Scand.* 82, 714–717.
- Podskochy, A., Gan, L., Fagerholm, P., 2000. Apoptosis in UV-exposed rabbit corneas. *Cornea* 19, 99–103.
- Rezaei Kanavi, M., Javadi, M.A., Zabihi Yeganeh, H.R., 2008. Corneal involvement in xeroderma pigmentosum; a histopathologic report. *J. Ophthalmic Vis. Res.* 3, 66–69.
- Ringvold, A., Davanger, M., Olsen, E.G., 1982. Changes of the cornea endothelium after ultraviolet radiation. *Acta Ophthalmol.* 60, 41–53.
- Shell, S.M., Li, Z., Shkriabai, N., Kvaratskhelia, M., Brosey, C., Serrano, M.A., Chazin, W. J., Musich, P.R., Zou, Y., 2009. Checkpoint kinase ATR promotes nucleotide excision repair of UV-induced DNA damage via physical interaction with xeroderma pigmentosum group A. *J. Biol. Chem.* 284, 24213–24222.
- Soufir, N., Ged, C., Bourillon, A., Austerlitz, F., Chemin, C., Sary, A., Armier, J., Pham, D., Khadir, K., Roume, J., Hadj-Rabia, S., Bouadjar, B., Taieb, A., de Verneuil, H., Benchiki, H., Grandchamp, B., Sarasin, A., 2010. A prevalent mutation with founder effect in xeroderma pigmentosum group C from north Africa. *J. Invest. Dermatol.* 130, 1537–1542.
- Volker, M., Mone, M.J., Karmakar, P., van Hoffen, A., Schul, W., Vermeulen, W., Soufir, N., Ged, C., Bourillon, A., Austerlitz, F., Chemin, C., Sary, A., Armier, J., Pham, D., Khadir, K., Roume, J., Hadj-Rabia, S., Bouadjar, B., Taieb, A., de Verneuil, H., Benchiki, H., Grandchamp, B., Sarasin, A., 2010. A prevalent mutation with founder effect in xeroderma pigmentosum group C from north Africa. *J. Invest. Dermatol.* 130, 1537–1542.
- Wu, X., Shell, S.M., Liu, Y., Zou, Y., 2007. ATR-dependent checkpoint modulates XPA nuclear import in response to UV irradiation. *Oncogene* 26, 757–764.
- Yam, J.C., Kwok, A.K., 2014. Ultraviolet light and ocular diseases. *Int. Ophthalmol.* 34, 383–400.
- Zhang, X.P., Liu, F., Cheng, Z., Wang, W., 2009. Cell fate decision mediated by p53 pulses. *Proc. Natl. Acad. Sci. U.S.A.* 106, 12245–12250.